Shear stress markedly alters the proteomic response to hypoxia in human pulmonary endothelial cells

Daria S. Kostyunina[1,2], Simon C. Rowan[1,2,3], Nikolai V. Pakhomov[1,2], Eugene Dillon[2], Keith D. Rochfort[4], Philip M. Cummins[5], Malachy J. O'Rourke[6], Paul McLoughlin[1,2]

1. School of Medicine, University College Dublin, Dublin, Ireland

2. Conway Institute, University College Dublin, Dublin, Ireland

3. Department of Medicine, Cedars-Sinai Medical Center, Los Angeles, United States of America

4. School of Nursing, Psychotherapy, and Community Health and the National Institute for Cellular Biotechnology, Dublin City University, Dublin, Ireland

5. School of Biotechnology and the National Institute for Cellular Biotechnology, Dublin City University, Dublin, Ireland

6. School of Mechanical and Materials Engineering, University College Dublin, Dublin, Ireland

Corresponding author

Paul McLoughlin paul.mcloughlin@ucd.ie

Author contributions

D.S.K. and P.McL. conceived the study. D.S.K., K.D.R., P.M.C., S.C.R, E.D., and P.McL contributed to the design of experiments. D.S.K., E.D., S.C.R., N.V.P., M.O'R. performed experiments and contributed to sample analysis including scRNAseq and computational fluid dynamics. D.S.K., S.C.R, N.V.P., E.D., M.O'R. and P.McL contributed to data presentation and the preparation of figures. D.S.K. and P.McL. drafted the manuscript. D.S.K., K.D.R., P.M.C., S.C.R, N.V.P., E.D., M.O'R. and P.McL contributed to data interpretation, editing and revision of the manuscript. All authors approved the final manuscript.

Funding

This work was funded by Science Foundation Ireland and University College Dublin. S.C.R. was supported by an EU Horizon 2020 Marie Skłodowska-Curie grant.

This article has an online data supplement, which is accessible from this issue's table of content online at www.atsjournals.org.

AJRCMB Articles in Press. Published February 02, 2023 as 10.1165/rcmb.2022-0340OC

Abstract

Blood flow produces shear stress that homeostatically regulates the phenotype of pulmonary endothelial cells exerting anti-inflammatory and anti-thrombotic actions and maintaining normal barrier function. Hypoxia due to diseases, such as COPD, causes vasoconstriction, increased vascular resistance and pulmonary hypertension. Hypoxia-induced changes in endothelial function play a central role in the development of pulmonary hypertension. However, the interactive effects of hypoxia and shear stress on the pulmonary endothelial phenotype have not been studied. Human pulmonary microvascular endothelial cells were cultured in normoxia or hypoxia while subjected to physiological shear stress or in static conditions. Unbiased proteomics was used to identify hypoxia-induced changes in protein expression. Using publicly available scRNAseq datasets, differences in gene expression between the alveolar endothelial cells from COPD and healthy lungs were identified. 60 proteins were identified whose expression changed in response to hypoxia in conditions of physiological shear stress but not in static conditions. These included proteins that are crucial for endothelial homeostasis e.g. JAM-A, ERG or implicated in pulmonary hypertension e.g. thrombospondin-1. 55 of these 60 have not been previously implicated in the development of hypoxic lung diseases. mRNA for five of the 60 (ERG, MCRIP1, EIF4A2, HSP90AA1 and DNAJA1) showed similar changes in the alveolar endothelial cells of COPD compared to healthy lungs in females but not in males. These data show that the proteomic responses of the pulmonary microvascular endothelium to hypoxia are significantly altered by shear stress and suggest that these shear-hypoxia interactions are important in the development of hypoxic pulmonary vascular disease.

Keywords

AJRCMB Articles in Press. Published February 02, 2023 as 10.1165/rcmb.2022-0340OC

Pulmonary microvascular endothelial cells, shear stress, hypoxia, COPD

AJRCMB Articles in Press. Published February 02, 2023 as 10.1165/rcmb.2022-0340OC

Introduction

Pulmonary endothelial cells *in vivo* constantly experience shear stress caused by blood flow. Shear stress regulates numerous signalling pathways and the expression of hundreds of genes in the endothelium (1). Unidirectional, laminar shear stress, as experienced by most endothelial cells under physiological conditions, induces endothelial cell elongation in the direction of flow, increases expression of vasodilator, anti-inflammatory, and anti-oxidative genes, and improves endothelial cell layer barrier function (1). The transcription factors Krüppel-like 2 and 4 (KLF2 and KLF4) play a central role in regulating the changes in gene expression in response to shear stress (1).

Alveolar hypoxia occurs in chronic lung diseases, the most common of which are chronic obstructive pulmonary disease (COPD), obstructive sleep apnoea and interstitial lung diseases (2). This alveolar hypoxia induces pulmonary artery vasoconstriction and remodelling which lead to the development of pulmonary hypertension (2). Pulmonary hypertension due to hypoxic lung diseases independently predicts increased morbidity and mortality (3).

Pulmonary endothelial cells play a crucial role in the vasoconstriction and vascular remodelling that lead to the development of pulmonary hypertension in response to alveolar hypoxia. Hypoxia also stimulates the development of a pro-inflammatory phenotype in the pulmonary endothelium (4). However, the endothelial cell responses to hypoxia *in vitro* have almost exclusively been examined under static conditions, in contrast to *in vivo* conditions in which they experience shear stress.

We hypothesised that physiological shear stress would alter the hypoxic responses of human pulmonary microvascular endothelial cells and that those responses would be similar to the responses of pulmonary endothelial cells to hypoxia *in vivo*. We compared the changes in the

AJRCMB Articles in Press. Published February 02, 2023 as 10.1165/rcmb.2022-0340OC

proteome of human pulmonary microvascular endothelial cells exposed to hypoxia under conditions of physiological shear stress *in vitro* to the changes detected in endothelial cells cultured in static conditions. We identified a set of hypoxia-induced changes in protein expression that were specific to cells under conditions of shear stress and examined the corresponding mRNA expression in the alveolar endothelial cells of COPD lungs using single cell RNA sequencing data. Some of the results of these studies have been previously reported in the form of an abstract (5).

Methods

Additional details are provided in the online data supplement.

Shear stress application

Human pulmonary microvascular endothelial cells (HPMEC, Promocell) from healthy male and female donors (53-70 years old) were exposed to shear stress, using an orbital shaker (SSM1, Stuart) (187 rotations per minute) and the relative viscosity of the cell culture medium was increased to 3.2 by addition of 7% Ficoll® PM400 (6). These conditions gave a shear stress of 10 dyn/cm^2 as calculated using an extended solution to Stokes' second problem (6, 7). After 24 hours in these normoxic conditions, cells were either placed into hypoxic conditions (1% O_2) or remained in normoxic conditions for a further 24 hours while shear stress continued. Separate cells were simultaneously cultured in standard static conditions in normoxia or hypoxia. Computational fluid dynamics (CFD) were used to characterise the applied shear stress in detail.

RT-qPCR

AJRCMB Articles in Press. Published February 02, 2023 as 10.1165/rcmb.2022-0340OC

TaqMan assays (Thermo Scientific) were used. Target gene expression was normalized to housekeeping gene (HPRT1). For statistical analysis normalized target gene expression was $\log_2$ transformed. P values were calculated using repeated measures ANOVA with Geisser-Greenhouse correction and followed by the Holm-Šídák's step-down test for pairwise comparisons (Prism 9, GraphPad).

ELISA

Interleukin 6 (IL-6) was measured in HPMEC supernatant using ELISA. P values were calculated using Friedman test with Dunn's multiple comparisons test.

Western Blotting

Proteins were separated by electrophoresis and transferred to polyvinylidene fluoride membranes. Specific proteins were labelled using appropriate primary and secondary antibodies and then detected using fluorescent labels. Target protein expression was normalized to β-actin. Data were $\log_2$ transformed and P values were calculated using a paired t-test.

Proteomics

HPMEC lysates were analysed using label-free quantitative mass spectrometry connected to a chromatography system. Raw data were processed using MaxQuant incorporating Andromeda (8, 9). Differentially expressed proteins were identified using Perseus software (ANOVA, permutation-based FDR, $q<0.05$). Pairwise comparisons were undertaken using Tukey's honestly significant difference test. Where expression of specific individual proteins was examined, P values were calculated using ANOVA and followed by the Holm-Šídák's step-

AJRCMB Articles in Press. Published February 02, 2023 as 10.1165/rcmb.2022-0340OC

down test for pairwise comparisons. Data are available via ProteomeXchange with identifier PXD036260.

Immunofluorescent imaging

HPMEC monolayers were fixed on six well plates and stained using primary anti-zonula occludens-1 antibodies. Images were acquired using a Zeiss confocal microscope with Airyscan. Identical settings were applied to acquire and display images from all four experimental conditions.

Single cell RNA sequencing

Pulmonary endothelial cells from male and female COPD patients and healthy donors were identified from four publicly available single cell RNA sequencing datasets (10–13). Analysis was undertaken using "Seurat". For the final analysis we identified the pulmonary endothelial cells from donors that were from an age range (50-76 years old) similar to that of the donors of the HPMEC used in our *in vitro* studies. Because COPD leads to alveolar hypoxia we focused on two types of alveolar endothelial cells (aerocytes and general capillary cells). Genes differentially expressed between healthy and COPD lungs were identified using Wilcoxon two sample test with Bonferroni correction (p-adjusted<0.05) and a $\log_2$ difference >0.6 (fold change >1.5).

Results

Shear stress characterisation

Using computational fluid dynamics (CFD) we characterised in detail the shear stress conditions experienced by the cells cultured on the orbital shaker (Figure 1). The mean

AJRCMB Articles in Press. Published February 02, 2023 as 10.1165/rcmb.2022-0340OC

magnitude of shear stress experienced by the HPMEC was 13.1 dyn/cm^2, i.e. approximately 31% greater than the value (10 dyn/cm^2) given by the commonly used extended solution to Stokes' second problem (6, 7) (Suppl. Table 1). It varied from 7 to 21 dyn/cm^2 at different points within the well (Figure 1A and 1B). These values lie within the range of the shear stress values predicted by recently published models for endothelial cells in the intact pulmonary microvasculature in the healthy lung (14, 15).

Previously it has been shown that a high oscillatory shear index (OSI > 0.2) induced a pro-inflammatory state in endothelial cells and that very high OSI (>0.4) caused increased permeability of the endothelial barrier (16, 17). We found that in the shear stress conditions we used, OSI was low (<0.2) on 91% of the well area, and only 0.25% of the well area in the center of the well experienced an OSI>0.4 (Figure 1C and 1D).

We compared the shear stress pattern produced by the high viscosity medium we used (relative viscosity 3.2) to that which cells would have experienced if we had used standard (low viscosity) cell culture medium (relative viscosity 1.1) combined with a higher rate of rotation (275 rotations per minute) to produce the same shear stress, calculated using the extended Stokes' solution i.e. the commonly used approach (6, 7). CFD demonstrated that use of standard medium would have substantially reduced the area of low OSI (<0.2) to 77% of the well (Suppl. Figure 1B; Suppl. Table 1). A further possible advantage of using the high viscosity medium was a significant reduction of the Reynolds and Froude numbers (Suppl. Table 1). Lower Reynolds and Froude numbers are associated with lower turbulence intensities. Normalized fluid velocities were plotted throughout one complete rotation for three radial locations (Figure 1E and 1F).

AJRCMB Articles in Press. Published February 02, 2023 as 10.1165/rcmb.2022-0340OC

Expression of the well-characterised shear responsive genes, endothelial nitric oxide synthase (eNOS) (1) and superoxide dismutase 1 (SOD1) (18), was increased in response to shear stress in both cells collected from whole well and cells collected from the periphery of the well alone (Figure 1G and 1H). Based on these results, all further experiments were undertaken on whole well lysates.

The effect of shear stress and hypoxia on shear-responsive genes and inflammatory markers

As we had designed our experimental conditions to produce a physiological response to shear stress, we examined changes in the expression of genes and proteins known to be increased in response to laminar flow conditions (1, 18). The shear-responsive transcription factors Kruppel-like factors 2 and 4 (KLF2 and KLF4) (1) were upregulated in response to shear stress in both normoxic and hypoxic conditions (Figure 2A and 2B). eNOS mRNA was upregulated in response to shear in normoxia and also in hypoxia (Figure 2C). However, a second shear-responsive gene, SOD1 (18), was upregulated in response to shear stress in normoxia but, interestingly, was not significantly changed in response to shear stress in hypoxia (Figure 2D). KLF2 and KLF4 proteins were not detected by mass spectrometric analysis. Mass spectrometric analysis showed that eNOS protein was upregulated in response to shear stress in both normoxic and hypoxic conditions (Figure 2E). SOD1 protein was statistically significantly upregulated in response to shear stress only in normoxia (Figure 2F). Taken together, these results confirmed classic shear stress-induced changes in pulmonary microvascular endothelial homeostatic genes and proteins (1, 18).

Endothelial inflammation was assessed by studying protein expression of intercellular adhesion molecule 1 (ICAM1) and secreted interleukin 6 (IL-6) in the culture medium (Figure

AJRCMB Articles in Press. Published February 02, 2023 as 10.1165/rcmb.2022-0340OC

2G and 2H). There were no differences in either of these inflammatory markers across the four experimental conditions, suggesting that neither the shear stress nor the hypoxic conditions caused an inflammatory phenotype.

The effect of shear stress on canonical responses to hypoxia

Next, we checked the regulators of the hypoxic response, hypoxia-inducible factors (HIF) proteins, and their targets (Figure 3). HIF-1α and HIF-2α proteins were not detectable in normoxia in either static or sheared conditions but were abundant in hypoxia (Figure 3, A and B). Both HIF-1α and HIF-2α proteins were reduced in sheared hypoxic conditions compared to static hypoxic conditions (Figure 3A and 3B). HIF1A mRNA expression was not reduced in sheared hypoxic compared to static hypoxic conditions (Figure 3A). Thus, the reduction of HIF1A protein expression in sheared hypoxic conditions compared to static hypoxic conditions was not caused by changes in gene transcription. HIF2A mRNA was also similar in static hypoxic and sheared hypoxic conditions and thus the reduction in HIF-2α protein expression observed in sheared hypoxic conditions must have been caused by mRNA-independent mechanisms (Figure 3B). Hypoxia induced a decrease of HIF1A mRNA in static conditions (Figure 3A), in agreement with previously published data (19). We found that a similar hypoxia-induced reduction of HIF1A and HIF2A mRNA was observed in sheared conditions (Figure 3A and 3B).

We also examined the well-known HIF regulated genes glucose transporter 1 (GLUT1) and vascular endothelial growth factor A (VEGFA) (20, 21) and confirmed that hypoxia induced upregulation of GLUT1 and VEGFA mRNA expression in static and sheared conditions (Figure 3C and 3E). Interestingly, GLUT1 mRNA and protein were also upregulated in response to

AJRCMB Articles in Press. Published February 02, 2023 as 10.1165/rcmb.2022-0340OC

shear stress in normoxia (Figure 3C and 3D). VEGFA protein was not detected by mass spectrometric analysis. However, another well-known HIF-responsive, pro-angiogenic protein, angiopoietin-like 4 (ANGPTL4) (21), showed a robust, hypoxia-induced increase in expression to similar levels in both static and sheared conditions (Figure 3F). The hypoxia-induced increase in expression of GLUT1, VEGFA and ANGPTL4 was not diminished in sheared conditions despite the decreased abundance of HIF-1α and HIF-2α proteins (Figure 3A and 3B). Taken together, these results confirmed classic hypoxia-induced changes in pulmonary microvascular endothelial gene and protein expression in both static and sheared conditions (20, 21).

Shear stress altered the proteomic response to hypoxia in HPMEC

The unbiased proteomics analysis detected 2192 proteins in total. Principal component analysis (PCA) was undertaken on proteomics data on the individual samples from the four experimental conditions (static normoxia, static hypoxia, shear normoxia and shear hypoxia) and revealed two clusters (Figure 4A). One cluster consisted of static samples, independent of whether they were normoxic or hypoxic, while all the sheared samples (both normoxic and hypoxic) were in the second cluster (Figure 4A).

We compared the four experimental conditions and identified 308 proteins whose expression was significantly different (ANOVA, FDR q value<0.05) and these are presented as a heatmap (Figure 4B). Among these 308 proteins we found 86 whose expression was significantly increased or decreased by hypoxia. Of these, 16 proteins changed similarly in response to hypoxia in both static and sheared conditions (Figure 4C and 4D, Suppl. Tables 2 and 3). 13 increased in response to hypoxia: ANGPTL4, solute carrier family 2 member 3 (SLC2A3) also

AJRCMB Articles in Press. Published February 02, 2023 as 10.1165/rcmb.2022-0340OC

known as facilitated glucose transporter 3 (GLUT3), protein tyrosine phosphatase receptor type B (PTPRB) also known as vascular endothelial protein tyrosine phosphatase, A-kinase anchoring protein 12 (AKAP12), lysyl oxidase like 2 (LOXL2), acireductone dioxygenase 1 (ADI1), succinate dehydrogenase complex flavoprotein subunit A (SDHA), cold inducible RNA binding protein (CIRBP), cellular communication network factor 2 (CCN2) also known as connective tissue growth factor (CTGF), AHNAK nucleoprotein (AHNAK), NADH:ubiquinone oxidoreductase core subunit S1 (NDUFS1), lactate dehydrogenase A (LDHA), S100 calcium binding protein A10 (S100A10) and three decreased in response to hypoxia: microtubule associated protein 1B (MAP1B), growth factor receptor bound protein 2 (GRB2), cysteine and histidine rich domain containing 1 (CHORDC) (Figure 4C and 4D, Suppl. Tables 2 and 3).

We identified 70 proteins whose responses to hypoxia were different in static and sheared conditions (Figure 5). Of these, 10 proteins changed in response to hypoxia in static conditions, but not in sheared conditions. Seven increased expression in response to hypoxia: breast cancer anti-estrogen resistance protein 1 isoform 1 (BCAR1), SH2 domain-containing protein 3C isoform c (SH2D3C), solute carrier family 2 member 1 (SLC2A1) also known as facilitated glucose transporter 1 (GLUT1), phosphoglycerate mutase 1 (PGAM1), fructose-bisphosphate aldolase C (ALDOC), Hemoglobin subunit alpha (HBA), Syntaxin-3 (STX3) and three reduced expression in response to hypoxia: ADP-ribosylation factor GTPase-activating protein 1 (ARFGAP1), Cytospin-A (SPECC1L), Delta-1-pyrroline-5-carboxylate synthase (ALDH18A1) (Figure 5A and 5B, Suppl. Tables 4 and 5).

In sheared conditions, 60 proteins changed in response to hypoxia but were not statistically significantly different between normoxia and hypoxia under static conditions (Figure 5C and 5D and Suppl. Tables 6 and 7). Of these, 17 proteins showed increased expression and 43

AJRCMB Articles in Press. Published February 02, 2023 as 10.1165/rcmb.2022-0340OC

proteins showed reduced expression in response to hypoxia. To illustrate more clearly this shear-dependent alteration of protein expression in response to hypoxia, scatter plots of two of these previously known to be important in endothelial function and vascular remodelling are shown (Figure 5E and 5F). Thrombospondin 1 (THBS1) protein increased in response to hypoxia only in sheared conditions (Figure 5E), while heat shock protein HSP 90-alpha isoform 1 (HSP90AA1) decreased in response to hypoxia only in sheared conditions (Figure 5F) (22–25). Taken together, these results demonstrate that the effect of hypoxia on the abundance of some proteins is different in HPMEC that are cultured under physiological shear stress conditions compared to standard static conditions.

We were interested to note that junctional adhesion molecule A (JAM-A), also known as F11R, was one of the proteins whose expression was reduced in response to hypoxia only in sheared conditions (Figure 6A). This protein is required for the normal formation and function of endothelial cell junctions (26–28). JAM-A mRNA changed in a similar way (reduced in hypoxia only in the presence of shear stress) suggesting that the reduction in protein was due to change in mRNA expression (Figure 6B). Because JAM-A regulates cells junctions, we examined tight junction protein (TJP1), also known as zonula occludens 1 (ZO-1), and VE-cadherin (CDH5) (Figure 6C-6G). ZO-1 and CDH5 protein expression increased in response to shear stress but neither mRNA was altered by shear stress (Figure 6C, 6D, 6E and 6F). Both CDH5 and ZO-1 were unchanged in hypoxia. Immunostaining of the cultured endothelial monolayer showed that in normoxia shear stress increased ZO-1 localization to the cell junction region compared to static conditions but that this shear-induced localization was markedly reduced in hypoxia (Figure 6G).

AJRCMB Articles in Press. Published February 02, 2023 as 10.1165/rcmb.2022-0340OC

Differentially expressed mRNAs in the alveolar endothelial cells of COPD lungs

Changes in protein expression in response to hypoxia in endothelial cells exposed to shear stress (16 that changed in response to hypoxia in both static and sheared conditions and 60 that changed in sheared conditions alone) may have been produced either by changes in gene expression or by post-transcriptional or by post-translational mechanisms. Thus, we expected that for some, but not all, of these 76 proteins corresponding changes in mRNA might be detected in endothelial cells that were hypoxic *in vivo*. To test this hypothesis, we compared single cell RNA sequencing data from healthy lungs and from the lungs of patients with COPD, which were obtained from publicly available data sets (10–13). Alveolar hypoxia is a characteristic feature of the lungs of patients with COPD (2).

We identified six different subtypes of endothelial cells (arterial, general capillary, aerocytes, pulmonary venous, systemic venous, and lymphatic endothelial cells) (Figure 7A and 7B). For further analysis we focused on the endothelial cells that are located in alveoli and thus are most directly exposed to alveolar hypoxia i.e. general capillary endothelial cells and aerocytes (29).

We next examined the single cell RNA sequencing data sets to identify differentially expressed genes in COPD capillary endothelial cells that coded for proteins that had changed expression in response to hypoxia in the cultured endothelial cells (Figure 7). Previously it has been reported that females have better survival with COPD than males (30). Because of this striking sex difference, we examined male and female data separately. The mRNAs of four proteins that were increased in hypoxia in both static and sheared pulmonary microvascular endothelial cells (SLC2A3, PTPRB, AHNAK and LOXL2) were increased significantly in the general capillary cells of female COPD lungs compared to female control lungs (Figure 7C).

AJRCMB Articles in Press. Published February 02, 2023 as 10.1165/rcmb.2022-0340OC

Three of these four genes (SLC2A3, AHNAK and LOXL2) were also significantly increased in the aerocytes of female COPD lungs.

Of the proteins whose expression was increased in response to hypoxia only when endothelial cells were exposed to sheared conditions, the encoding mRNAs for ETS transcription factor ERG (ERG) and MAPK regulated corepressor interacting protein 1 (MCRIP1) were upregulated in the general capillary endothelial cells of female COPD lung samples (Figure 7D). In the aeroctyes of female COPD lungs ERG mRNA was also significantly increased (Figure 7D).

There were three genes that were significantly downregulated in both general capillary cells and in the aerocytes of female COPD samples whose corresponding proteins were reduced in HPMEC in response to hypoxia only in sheared conditions: eukaryotic translation initiation factor 4A2 (EIF4A2), HSP90AA1 and DnaJ heat shock protein family (Hsp40) member A1 (DNAJA1) (Figure 7E).

No statistically significant differences in the expression of these mRNAs (encoding proteins that had changed expression in response to hypoxia in the cultured endothelial cells) between healthy and COPD endothelial cells were detected in males (Figure 7C, 7D and 7E).

Discussion

The work reported here was undertaken to examine the hypoxic responses of human pulmonary microvascular endothelial cells under conditions of continuous shear stress since *in vivo* these cells are exposed throughout life to blood flow-induced shear stress. Our results show for the first time that the proteomic response of the human pulmonary microvascular endothelium to hypoxia is significantly altered in the presence of physiological shear stress.

AJRCMB Articles in Press. Published February 02, 2023 as 10.1165/rcmb.2022-0340OC

For our *in vitro* experiments, we aimed to expose the pulmonary endothelial cells to shear stress that was representative of that which endothelial cells experience *in vivo*. However, direct measurement of the wall shear stress in the arterioles, capillaries and venules of the pulmonary circulation has not been made to date. Direct determination of wall shear stress *in vivo* in the systemic microcirculation using microviscometric technique showed that the wall shear stress was in the range of 5-10 dyn/cm^2 (31). Wall shear stress, predicted on the basis of a number of different mathematical models, varies extensively, reflecting the differing assumptions and simplifications incorporated into such models (14, 15, 32–34). Given these uncertainties, we chose our experimental conditions so that the endothelium would show physiological features of a healthy endothelial monolayer. We have previously shown that shear stress similar to that used in the present study (i.e. 10 dyn/cm^2 predicted by an extended solution to Stokes' second problem), achieved using high viscosity culture medium, improved barrier function in a pulmonary endothelial monolayer when compared to lower shear stress conditions (6). In a series of preliminary experiments (data not shown), we increased the shear stress to a higher value (14 dyn/cm^2 as predicted by an extended solution to Stokes' second problem) and observed significant loss of cells due to their detachment leaving visible defects in the monolayer. Based on these considerations, we chose the value of 10 dyn/cm^2 for the current investigations. Our finding of the increased expression of markers that are well-known to be upregulated in response to protective shear stress (KLF2, KLF4, NOS3 and SOD1) provides evidence of the homeostatic, protective nature of the shear stress we used and demonstrate that these conditions induced a more physiological phenotype in the cells than those cultured under static conditions (1). This agrees well with previous reports of improved endothelial barrier function following exposure

AJRCMB Articles in Press. Published February 02, 2023 as 10.1165/rcmb.2022-0340OC

to shear stress induced by orbital rotation in the endothelial cells from other vascular beds (35).

We first checked the effects of shear stress on the canonical regulators of hypoxic responses, hypoxia-inducible factors (HIF) proteins, and their targets (20). HIF-1α and HIF-2α proteins were reduced in sheared conditions independently of changes in their mRNAs, possibly by post-translational mechanisms (Figure 3), in keeping with previous reports of post-translational regulation of HIF protein abundance (36). Interestingly, despite the shear stress induced decrease in hypoxic accumulation of HIF-1α and HIF-2α, some of their well-known mRNA targets, for example GLUT1 and VEGFA (20), were increased to the same extent as in static conditions (Figure 3C and 3E).

As was anticipated, the proteomic analysis identified increases in the expression of proteins that are well recognised as hypoxia responsive under static conditions, such as GLUT1, ANGPTL4, LDHA, ALDOC, confirming the validity of our experimental model (20, 21) (Figure 3D and 3F, Figure 4C and Figure 5A). However, we also found that 60 proteins were changed in response to hypoxia in sheared but not static conditions, changes that would not have been detected if hypoxic responses had only been examined under the static conditions commonly used in *in vitro* models. A number of these 60 proteins have previously been shown to be hypoxia-responsive in other cells and tissues e.g. SERPINE1, cellular communication network factor 1 (CCN1), RNA-binding protein 3 (RBM3), THBS1, tyrosine-protein kinase CSK also known as C-terminal Src kinase (CSK), JAM-A, HSP90AA1, Ras GTPase-activating protein 1 (RASA1), Heat shock 70 kDa protein 1B (HSPA1B, also known as HSP70-2), Heat shock 70 kDa protein 12B (HSPA12B) and plasma membrane calcium-transporting ATPase 4 (ATP2B4). However, none of these has previously been identified as hypoxia responsive in pulmonary

AJRCMB Articles in Press. Published February 02, 2023 as 10.1165/rcmb.2022-0340OC

microvascular endothelial cells (37–46). Only two of the 60 proteins, CCN1 and THBS1, which were among those increased in hypoxia only in sheared conditions, have been previously reported to increase in hypoxic lungs *in vivo* and in hypoxic endothelial cells from large pulmonary arteries (22, 23, 38). The identification of these two proteins with known roles in the development of vascular disease among those altered by hypoxia only in the presence of shear stress supports the view that this *in vitro* model recapitulates important physiological mechanisms activated in the hypoxic pulmonary endothelium *in vivo*.

Of the 17 proteins increased by hypoxia only in sheared conditions, 15 have not previously been identified as hypoxia responsive in pulmonary vascular endothelial cells. Of the 43 proteins that we identified as reduced by hypoxia only in sheared conditions (Figure 5D), five (CSK, HSP90AA1, HSPA1B, ATP2B4, HSPA12B) were previously shown to be increased in response to hypoxia in other cells types i.e. a changed in the opposite direction to that which we found (40, 42, 44–46). Of these 43 proteins (Figure 5D) 41 have not previously been implicated in the development of hypoxic lung diseases. Taken together, these finding show that the hypoxic responses of the pulmonary microvascular endothelium are substantially altered in the presence of shear stress and are very different from previously reported hypoxia responses in other cell types. This suggests that the hypoxia-shear stress interaction is central to the unique responses of the pulmonary circulation to hypoxia *in vivo*, including hypoxia-induced increase in vascular resistance (47).

It is particularly interesting to note that our results identified reduction of expression of proteins known to be essential for normal vascular homeostasis in systemic endothelial cells although these have not previously been shown to be hypoxia responsive in the pulmonary microvascular endothelium, for example JAM-A, Ephrin-B1 (EFNB1) and Prelamin-A/C (LMNA)

AJRCMB Articles in Press. Published February 02, 2023 as 10.1165/rcmb.2022-0340OC

(26, 48, 49). We examined JAM-A further as it is required to maintain normal endothelial barrier permeability in the systemic circulation (26, 28). This was of particular interest given that increased endothelial permeability is a key step in the development of both hypoxia-induced pulmonary edema and hypoxic pulmonary hypertension (50, 51). It has previously been shown that reduction of JAM-A in dermal capillary endothelial cells leads to movement of ZO-1 out of the endothelial tight junctions into the cytosol thus causing increased endothelial permeability (26). These reports taken together with our findings that hypoxia in shear stress conditions caused reduction of JAM-A expression and loss of ZO-1 from pulmonary endothelial junctions suggest that this mechanism could contribute to hypoxia-induced increases in pulmonary vascular permeability and thus to the development of lung diseases.

The data comparing alveolar capillary endothelial cells of COPD lungs to those of normal lungs provide strong supporting evidence for the pathophysiological relevance of the proteins identified *in vitro* as hypoxia responsive. As expected, this was a subset of the list of the hypoxia responsive proteins since among them there must be proteins that were altered by post-translational mechanisms. In addition, since the single cell RNA sequencing analysis was undertaken on all lung cells and endothelial cells were not the focus of those studies, there were relatively few endothelial cells in the data sets (10–13). Nonetheless, the differentially expressed genes code for proteins that are known to be hypoxia responsive and proteins that have important functions within the vasculature.

In females, mRNAs encoding nine of the proteins identified in the *in vitro* proteomic data set were differentially expressed. Four of these were upregulated in both static and sheared conditions and three of these four have previously been shown to play a role in endothelial

AJRCMB Articles in Press. Published February 02, 2023 as 10.1165/rcmb.2022-0340OC

homeostasis and angiogenesis in systemic organs, although not in the lungs. SCL2A3 (GLUT3) is a hypoxia responsive gene whose increased expression in the aortic endothelium promotes endothelial cell motility (52). LOXL2 is also expressed in the systemic endothelium and is known to be hypoxia responsive (53). It is required for angiogenesis, playing a role in the formation of the basement membrane (53). PTPRB is an hypoxia regulated, endothelial-specific receptor-type tyrosine phosphatase essential for angiogenesis and normal shear stress induced endothelial alignment (54).

The finding in the single cell RNA sequencing analysis of lung samples from females with COPD that a group of mRNAs in capillary endothelial cells, which coded for proteins changed by hypoxia only under shear stress, were similarly altered (reduced or increased) in COPD lungs compared to healthy lungs provides further support for the relevance of our findings to hypoxic lung disease. For the reasons outlined above, this is a subset of the list of 60 proteins. Nonetheless, it is notable that among these was ERG, a transcription factor essential for the maintenance of normal endothelial barrier function and vascular stability in healthy endothelium (55). Included in the genes whose expression was reduced, there was one that is required for normal endothelial cell homeostasis, HSP90AA1. In endothelial cells HSP90AA1 is essential for the normal function of eNOS and VEGFR2 (24, 25). Reduction in the expression of these homeostatic genes and proteins could therefore have contributed to altered vascular function in COPD, although further research will be required in the future to investigate this directly as these genes have not previously been identified as hypoxia responsive in the pulmonary microvascular endothelium.

Intriguingly, the differences in gene expression between healthy and COPD female samples contrasted markedly with the absence of significant differences in expression observed

AJRCMB Articles in Press. Published February 02, 2023 as 10.1165/rcmb.2022-0340OC

between healthy and COPD male samples. For some mRNAs the difference in expression between control male samples and samples from male COPD lungs seems to follow the same pattern as the differences between the female control and COPD lungs. The absence of statistically significant differences may reflect a lack of statistical power due to the smaller number of cells identified in male lungs e.g. aerocytes (Figure 7C and 7D). However, for the mRNAs coding for proteins that were reduced only in sheared conditions the pattern of differential expression between healthy and COPD lungs suggests a sex different response in both general capillary cells and aerocytes (Figure 7E). The presence of sex differences *in vivo* that we did not observe *in vitro* may be due to differences in the sex hormones or due to the influence of other cells in the intact lungs on the pulmonary endothelium (56). Further work will be required specifically designed to assess sex differences in the response of these genes and proteins in the lungs.

In this work we have shown that physiological shear stress alters the response to hypoxia in human pulmonary microvascular endothelial cells. We identified 60 proteins whose expression was significantly changed in response to hypoxia only in sheared conditions. Importantly, 55 of these have not previously been reported to be hypoxia responsive in the lung and have not been previously linked to hypoxic lung diseases. These changes would not have been detected if cells had only been examined in the more commonly used static culture conditions. Thus, in order to gain insights that are directly relevant to the role of hypoxic responses of endothelial cells *in vivo*, future work should include *in vitro* models that expose endothelial cells to shear stress. The *in vivo* relevance of the identified changes in the context of hypoxic lung disease is supported by our finding that for a sub-set of these proteins the encoding mRNA was similarly changed in the alveolar endothelial cells of COPD lungs in females. Taken together, these results suggest that the interactions of shear stress and

AJRCMB Articles in Press. Published February 02, 2023 as 10.1165/rcmb.2022-0340OC

hypoxia are central in the development of the vascular abnormalities characteristic of hypoxic lung diseases.

Acknowledgements

The authors thank Dr. Dimitri Scholz for help with immunofluorescent imaging and Dr. Vadim Zhernovkov for help with interpretation of proteomics analysis. Some of the results of these studies have been reported in the form of a thesis.

References

1. Wu D, Birukov K. Endothelial Cell Mechano-Metabolomic Coupling to Disease States in the Lung Microvasculature. *Front Bioeng Biotechnol* 2019;7:1–18.

2. Rowan SC, Keane MP, Gaine S, McLoughlin P. Hypoxic pulmonary hypertension in chronic lung diseases: Novel vasoconstrictor pathways. *Lancet Respir Med* 2016;4:225–236.

3. Zeder K, Avian A, Bachmaier G, Douschan P, Foris V, Sassmann T, Troester N, Brcic L, Fuchsjaeger M, Marsh LM, Maron BA, Olschewski H, Kovacs G. Elevated pulmonary vascular resistance predicts mortality in COPD patients. *Eur Respir J* 2021;58:4–7.

4. Fröhlich S, Boylan J, Mcloughlin P. Hypoxia-induced inflammation in the lung: A potential therapeutic target in acute lung injury? *Am J Respir Cell Mol Biol* 2013;48:271–279.

5. Kostyunina D, Rochfort KD, Cummins PM, McLoughlin P. The Hypoxic Response of Shear Aligned Endothelial Cells: Approaching In Vivo Conditions. 2020;A3879–A3879.doi:10.1164/ajrccm-conference.2020.201.1_meetingabstracts.a3879.

6. Rowan SC, Rochfort KD, Piouceau L, Cummins PM, O'Rourke M, McLoughlin P. Pulmonary endothelial permeability and tissue fluid balance depend on the viscosity of the perfusion solution. *Am J Physiol Cell Mol Physiol* 2018;315:L476–L484.

7. Ley K, Lundgren E, Berger E, Arfors K. Shear-dependent inhibition of granulocyte adhesion to cultured endothelium by dextran sulfate. *Blood* 1989;73:1324–1330.

8. Cox J, Mann M. MaxQuant enables high peptide identification rates, individualized p.p.b.-range mass accuracies and proteome-wide protein quantification. *Nat Biotechnol* 2008;26:1367–1372.

9. Cox J, Neuhauser N, Michalski A, Scheltema RA, Olsen J V., Mann M. Andromeda: A peptide search engine integrated into the MaxQuant environment. *J Proteome Res* 2011;10:1794–1805.

10. Valenzi E, Bulik M, Tabib T, Morse C, Sembrat J, Trejo Bittar H, Rojas M, Lafyatis R. Single-cell analysis reveals fibroblast heterogeneity and myofibroblasts in systemic sclerosis-associated interstitial lung disease. *Ann Rheum Dis* 2019;78:1379–1387.

11. Morse C, Tabib T, Sembrat J, Buschur KL, Bittar HT, Valenzi E, Jiang Y, Kass DJ, Gibson K, Chen W, Mora A, Benos P V., Rojas M, Lafyatis R. Proliferating SPP1/MERTK-expressing macrophages in idiopathic pulmonary fibrosis. *Eur Respir J* 2019;54:.

12. Adams TS, Schupp JC, Poli S, Ayaub EA, Neumark N, Ahangari F, Chu SG, Raby BA, DeIuliis G, Januszyk M, Duan Q, Arnett HA, Siddiqui A, Washko GR, Homer R, Yan X, Rosas IO, Kaminski N. Single-cell RNA-seq reveals ectopic and aberrant lung-resident cell populations in idiopathic pulmonary fibrosis. *Sci Adv* 2020;6:.

13. Reyfman PA, Walter JM, Joshi N, Anekalla KR, McQuattie-Pimentel AC, Chiu S, Fernandez R, Akbarpour M, Chen CI, Ren Z, Verma R, Abdala-Valencia H, Nam K, Chi M, Han SH, Gonzalez-Gonzalez FJ, Soberanes S, Watanabe S, Williams KJN, Flozak AS, Nicholson TT, Morgan VK, Winter DR, Hinchcliff M, Hrusch CL, Guzy RD, Bonham CA,

AJRCMB Articles in Press. Published February 02, 2023 as 10.1165/rcmb.2022-0340OC

Sperling AI, Bag R, *et al.* Single-cell transcriptomic analysis of human lung provides insights into the pathobiology of pulmonary fibrosis. *Am J Respir Crit Care Med* 2019;199:1517–1536.

14. Bartolo MA, Qureshi MU, Colebank MJ, Chesler NC, Olufsen MS. Numerical predictions of shear stress and cyclic stretch in pulmonary hypertension due to left heart failure. *Biomech Model Mechanobiol* 2022;21:363–381.

15. Yang W, Dong M, Rabinovitch M, Chan FP, Marsden AL, Feinstein JA. Evolution of hemodynamic forces in the pulmonary tree with progressively worsening pulmonary arterial hypertension in pediatric patients. *Biomech Model Mechanobiol* 2019;18:779–796.

16. Ghim M, Pang KT, Arshad M, Wang X, Weinberg PD. A novel method for segmenting growth of cells in sheared endothelial culture reveals the secretion of an anti-inflammatory mediator. *J Biol Eng* 2018;12:1–13.

17. Ghim M, Alpresa P, Yang SW, Braakman ST, Gray SG, Sherwin SJ, Van Reeuwijk M, Weinberg PD. Visualization of three pathways for macromolecule transport across cultured endothelium and their modification by flow. *Am J Physiol - Hear Circ Physiol* 2017;313:H959–H973.

18. Inoue N, Ramasamy S, Fukai T, Nerem RM, Harrison DG. Shear stress modulates expression of Cu/Zn superoxide dismutase in human aortic endothelial cells. *Circ Res* 1996;79:32–37.

19. Chamboredon S, Ciais D, Desroches-Castan A, Savid P, Bono F, Feige JJ, Cherradi N. Hypoxia-inducible factor-1α mRNA: A new target for destabilization by tristetraprolin in endothelial cells. *Mol Biol Cell* 2011;22:3366–3378.

20. Kierans SJ, Taylor CT. Regulation of glycolysis by the hypoxia-inducible factor (HIF): implications for cellular physiology. *J Physiol* 2021;599:23–37.

21. Le Jan S, Amy C, Cazes A, Monnot C, Lamandé N, Favier J, Philippe J, Sibony M, Gasc JM, Corvol P, Germain S. Angiopoietin-like 4 is a proangiogenic factor produced during ischemia and in conventional renal cell carcinoma. *Am J Pathol* 2003;162:1521–1528.

22. Rogers NM, Ghimire K, Calzada MJ, Isenberg JS. Matricellular protein thrombospondin-1 in pulmonary hypertension: Multiple pathways to disease. *Cardiovasc Res* 2017;113:858–868.

23. Kaiser R, Frantz C, Bals R, Wilkens H. The role of circulating thrombospondin-1 in patients with precapillary pulmonary hypertension. *Respir Res* 2016;17:4–13.

24. Averna M, Stifanese R, De Tullio R, Passalacqua M, Salamino F, Pontremoli S, Melloni E. Functional role of HSP90 complexes with endothelial nitric-oxide synthase (eNOS) and calpain on nitric oxide generation in endothelial cells. *J Biol Chem* 2008;283:29069–29076.

25. Le Boeuf F, Houle F, Huot J. Regulation of vascular endothelial growth factor receptor 2-mediated phosphorylation of focal adhesion kinase by heat shock protein 90 and Src kinase activities. *J Biol Chem* 2004;279:39175–39185.

AJRCMB Articles in Press. Published February 02, 2023 as 10.1165/rcmb.2022-0340OC

26. Tornavaca O, Chia M, Dufton N, Almagro LO, Conway DE, Randi AM, Schwartz MA, Matter K, Balda MS. ZO-1 controls endothelial adherens junctions, cell-cell tension, angiogenesis, and barrier formation. *J Cell Biol* 2015;208:821–838.

27. Fukuhara T, Kim J, Hokaiwado S, Nawa M, Okamoto H, Kogiso T, Watabe T, Hattori N. A novel immunotoxin reveals a new role for CD321 in endothelial cells. *PLoS One* 2017;12:1–12.

28. Kakogiannos N, Ferrari L, Giampietro C, Scalise AA, Maderna C, Ravà M, Taddei A, Lampugnani MG, Pisati F, Malinverno M, Martini E, Costa I, Lupia M, Cavallaro U, Beznoussenko G V., Mironov AA, Fernandes B, Rudini N, Dejana E, Giannotta M. JAM-A Acts via C/EBP-α to Promote Claudin-5 Expression and Enhance Endothelial Barrier Function. *Circ Res* 2020;127:1056–1073.

29. Gillich A, Zhang F, Farmer CG, Travaglini KJ, Tan SY, Gu M, Zhou B, Feinstein JA, Krasnow MA, Metzger RJ. Capillary cell-type specialization in the alveolus. *Nature* 2020;586:785–789.

30. De Torres JP, Cote CG, López M V., Casanova C, Díaz O, Marin JM, Pinto-Plata V, De Oca MM, Nekach H, Dordelly LJ, Aguirre-Jaime A, Celli BR. Sex differences in mortality in patients with COPD. *Eur Respir J* 2009;33:528–535.

31. Long DS, Smith ML, Pries AR, Ley K, Damiano ER. Microviscometry reveals reduced blood viscosity and altered shear rate and shear stress profiles in microvessels after hemodilution. *Proc Natl Acad Sci U S A* 2004;101:10060–10065.

32. Ghorishi Z, Milstein JM, Poulain FR, Moon-Grady A, Tacy T, Bennett SH, Fineman JR, Eldridge MW. Shear stress paradigm for perinatal fractal arterial network remodeling in lambs with pulmonary hypertension and increased pulmonary blood flow. *Am J Physiol - Hear Circ Physiol* 2007;292:3006–3018.

33. Allen RP, Schelegle ES, Bennett SH. Diverse forms of pulmonary hypertension remodel the arterial tree to a high shear phenotype. *Am J Physiol - Hear Circ Physiol* 2014;307:405–417.

34. Postles A, Clark AR, Tawhai MH. Dynamic blood flow and wall shear stress in pulmonary hypertensive disease. *2014 36th Annu Int Conf IEEE Eng Med Biol Soc EMBC 2014* 2014;5671–5674.doi:10.1109/EMBC.2014.6944914.

35. Warboys CM, Berson RE, Mann GE, Pearson JD, Weinberg PD. Acute and chronic exposure to shear stress have opposite effects on endothelial permeability to macromolecules. *Am J Physiol - Hear Circ Physiol* 2010;298:1850–1856.

36. Albanese A, Daly LA, Mennerich D, Kietzmann T, Sée V. The role of hypoxia-inducible factor post-translational modifications in regulating its localisation, stability, and activity. *Int J Mol Sci* 2021;22:1–18.

37. Qin Y, Zhang J, Babapoor-Farrokhran S, Applewhite B, Deshpande M, Megarity H, Flores-Bellver M, Aparicio-Domingo S, Ma T, Rui Y, Tzeng SY, Green JJ, Canto-Soler MV, Montaner S, Sodhi A. PAI-1 is a vascular cell-specific HIF-2-dependent angiogenic factor that promotes retinal neovascularization in diabetic patients. *Sci Adv* 2022;8:1–17.

AJRCMB Articles in Press. Published February 02, 2023 as 10.1165/rcmb.2022-0340OC

38. Lee SJ, Zhang M, Hu K, Lin L, Zhang D, Jin Y. CCN1 suppresses pulmonary vascular smooth muscle contraction in response to hypoxia. *Pulm Circ* 2015;5:716–722.

39. Wellmann S, Bührer C, Moderegger E, Zelmer A, Kirschner R, Koehne P, Fujita J, Seegar K. Oxygen-regulated expression of the RNA-binding proteins RBM3 and CIRP by a HIF-1-independent mechanism. *J Cell Sci* 2004;117:1785–1794.

40. Guo Q, Lu L, Liao Y, Wang X, Zhang Y, Liu Y, Huang S, Sun H, Li Z, Zhao L. Influence of c-Src on hypoxic resistance to paclitaxel in human ovarian cancer cells and reversal of FV-429. *Cell Death Dis* 2018;8:1–11.

41. Kakuki T, Kurose M, Takano K ichi, Kondoh A, Obata K, Nomura K, Miyata R, Kaneko Y, Konno T, Takahashi S, Hatakeyama T, Kohno T, Himi T, Kojima T. Dysregulation of junctional adhesion molecule-A via p63/GATA-3 in head and neck squamous cell carcinoma. *Oncotarget* 2016;7:33887–33900.

42. Santos EM, Fraga CA de C, Xavier ARE de O, Xavier MA de S, Souza MG, Jesus SF de, Paula AMB de, Farias LC, Santos SHS, Santos TG, Beraldo FH, Guimarães ALS. Prion protein is associated with a worse prognosis of head and neck squamous cell carcinoma. *J Oral Pathol Med* 2021;50:985–994.

43. Du C, Weng X, Hu W, Lv Z, Xiao H, Ding C, Gyabaah OAK, Xie H, Zhou L, Wu J, Zheng S. Hypoxia-inducible MiR-182 promotes angiogenesis by targeting RASA1 in hepatocellular carcinoma. *J Exp Clin Cancer Res* 2015;34:1–9.

44. Huang WJ, Xia LM, Zhu F, Huang B, Zhou C, Zhu HF, Wang B, Chen B, Lei P, Shen GX, Tian DA. Transcriptional upregulation of HSP70-2 by HIF-1 in cancer cells in response to hypoxia. *Int J Cancer* 2009;124:298–305.

45. Fan M, Yang K, Wang X, Wang Y, Tu F, Ha T, Liu L, Williams DL, Li C. Endothelial cell HSPA12B and yes-associated protein cooperatively regulate angiogenesis following myocardial infarction. *JCI Insight* 2020;5:1–18.

46. Deng L, Chen J, Wang T, Chen B, Yang L, Liao J, Chen Y, Wang J, Tang H, Yi J, Kang K, Li L, Gou D. PDGF/MEK/ERK axis represses Ca2+clearance via decreasing the abundance of plasma membrane Ca2+pump PMCA4 in pulmonary arterial smooth muscle cells. *Am J Physiol - Cell Physiol* 2021;320:C66–C79.

47. Costello CM, Howell K, Cahill E, McBryan J, Konigshoff M, Eickelberg O, Gaine S, Martin F, McLoughlin P. Lung-selective gene responses to alveolar hypoxia: potential role for the bone morphogenetic antagonist gremlin in pulmonary hypertension. *Am J Physiol Cell Mol Physiol* 2008;295:L272–L284.

48. Sun S, Qin W, Tang X, Meng Y, Hu W, Zhang S, Qian M, Liu Z, Cao X, Pang Q, Zhao B, Wang Z, Zhou Z, Liu B. Vascular endothelium–targeted Sirt7 gene therapy rejuvenates blood vessels and extends life span in a Hutchinson-Gilford progeria model. *Sci Adv* 2020;6:1–11.

49. Liu H, Devraj K, Möller K, Liebner S, Hecker M, Korff T. EphrinB-mediated reverse signalling controls junctional integrity and pro-inflammatory differentiation of endothelial cells. *Thromb Haemost* 2014;112:151–163.

50. She J, Goolaerts A, Shen J, Bi J, Tong L, Gao L, Song Y, Bai C. KGF-2 targets alveolar

AJRCMB Articles in Press. Published February 02, 2023 as 10.1165/rcmb.2022-0340OC

epithelia and capillary endothelia to reduce high altitude pulmonary oedema in rats. *J Cell Mol Med* 2012;16:3074–3084.

51. Zhou W, Liu K, Zeng L, He J, Gao X, Gu X, Chen X. Targeting VEGF-A/VEGFR2 Y949 Signaling-Mediated Vascular Permeability Alleviates Hypoxic Pulmonary Hypertension. *Circulation* 2022;146:1855–1881.

52. Wu D, Harrison DL, Szasz T, Yeh CF, Shentu TP, Meliton A, Huang RT, Zhou Z, Mutlu GM, Huang J, Fang Y. Single-cell metabolic imaging reveals a SLC2A3-dependent glycolytic burst in motile endothelial cells. *Nat Metab* 2021;3:714–727.

53. Bignon M, Pichol-Thievend C, Hardouin J, Malbouyres M, Bréchot N, Nasciutti L, Barret A, Teillon J, Guillon E, Etienne E, Caron M, Joubert-Caron R, Monnot C, Ruggiero F, Muller L, Germain S. Lysyl oxidase-like protein-2 regulates sprouting angiogenesis and type IV collagen assembly in the endothelial basement membrane. *Blood* 2011;118:3979–3989.

54. Winderlich M, Keller L, Cagna G, Broermann A, Kamenyeva O, Kiefer F, Deutsch U, Nottebaum AF, Vestweber D. VE-PTP controls blood vessel development by balancing Tie-2 activity. *J Cell Biol* 2009;185:657–671.

55. Shah A V., Birdsey GM, Peghaire C, Pitulescu ME, Dufton NP, Yang Y, Weinberg I, Osuna Almagro L, Payne L, Mason JC, Gerhardt H, Adams RH, Randi AM. The endothelial transcription factor ERG mediates Angiopoietin-1-dependent control of Notch signalling and vascular stability. *Nat Commun* 2017;8:1–16.

56. Kostyunina DS, McLoughlin P. Sex dimorphism in pulmonary hypertension: The role of the sex chromosomes. *Antioxidants* 2021;10:779.

AJRCMB Articles in Press. Published February 02, 2023 as 10.1165/rcmb.2022-0340OC

Figure legends

Figure 1. Characterization of shear stress on an endothelial monolayer within a single well (in a six well plate) during rotation on an orbital shaker together with the effects on shear responsive gene expression (rotation frequency - 187 rotations per minute, radius of gyration - 0.8 cm, radius of well - 1.75 cm, medium volume - 4 ml, medium relative viscosity - 3.23, medium density 1023 kg/m^3). (A) Schematic representation of the magnitude and direction of shear stress vectors throughout the base of the well. (B) Mean magnitude of wall shear stress (red curve) and mean wall shear stress (blue curve) throughout a single complete rotation plotted against radial distance from the well centre. (C) Color-coded representation showing the Oscillatory Shear Index (OSI) throughout the base of the well. (D) Oscillatory Shear Index (OSI) plotted against radial distance from the well centre. (E) Color-coded representation of normalized fluid velocities at a single time point at the base of the well (0.06 mm above the endothelial cell surface). (F) Normalized fluid velocities at 10% (r/R =0.10), 50% (r/R =0.50), and 70% (r/R=0.70) of the radius of the well throughout one complete orbit. (G and H) Expression of the shear-responsive genes eNOS and SOD1 in HPMEC collected from the whole area of the base of the well and in HPMEC collected from the periphery of the well alone (HPMEC from the central 40% of the basal well area were removed) after shear stress (72 hours) in normoxia. Target gene expression was normalised to housekeeping gene (HPRT1) expression in each sample. Data are presented as mean (SD), each symbol represents an individual donor. Solid symbols represent HPMEC from female donors, open symbols represent HPMEC from male donors. Values were $\log_2$ transformed for calculation of P values (repeated measures ANOVA followed by the Holm-Šídák's step-down test for pairwise comparisons). *p value <0.05.

Figure 2. Shear-responsive genes (A) KLF2, (B) KLF4, (C) eNOS, (D) SOD1, shear-responsive proteins (E) eNOS, (F) SOD1 and inflammatory markers (G) ICAM1 and (H) IL-6 after exposure to shear stress in normoxia (Norm, 21% O_2) or hypoxia (Hypo, 1% O_2) for 24 hours. For target genes expression (A-D) was normalised to housekeeping gene (HPRT1) expression in each sample. Values were $\log_2$ transformed for calculation of P values (repeated measures ANOVA followed by the Holm-Šídák's step-down test for pairwise comparisons). Protein expression (E-G) was quantified by mass spectrometric analysis. LFQ, label-free quantification. P values were calculated using ANOVA and followed by the Holm-Šídák's step-down test for pairwise comparisons. (#) indicates that in this experimental group this protein was not detected in one of the subjects. (F) IL-6 secreted by HPMEC and measured in supernatant. P values were calculated using Friedman test with Dunn's multiple comparisons test. Data are presented as mean (SD), each symbol represents an individual donor. Solid symbols represent HPMEC from female donors, open symbols represent HPMEC from male donors. *p value <0.05.

Figure 3. (A-B) Hypoxia (1% O_2 for 24 hours) induced accumulation of (A) HIF-1α and (B) HIF-2α proteins that was reduced by shear stress, although HIF-1α and HIF-2α (EPAS1) mRNA were not altered by shear stress. Representative immunoblots of HIF-1α and HIF-2α protein

AJRCMB Articles in Press. Published February 02, 2023 as 10.1165/rcmb.2022-0340OC

abundance for one donor are shown. Plots show values (western blotting) for five donors in each condition presented as percentages of the mean value of the "Static Hypoxia" group. For statistical analysis of western blotting data values were log_2 transformed and P values were calculated using a paired t-test. Expression of hypoxia-responsive genes (C) GLUT1, (E) VEGFA and proteins (D) GLUT1 and (F) ANGPTL4 in HPMEC after exposure to shear stress in normoxia (Norm, 21% O_2) or hypoxia (Hypo, 1% O_2) for 24 hours. For (C and E) values were log_2 transformed for calculation of P values (repeated measures ANOVA followed by the Holm-Šídák's step-down test for pairwise comparisons). Protein expression (D, F) was quantified by mass spectrometric analysis. P values were calculated using ANOVA and followed by the Holm-Šídák's step-down test for pairwise comparisons. Data are presented as mean (SD), each symbol represents an individual donor. Solid symbols represent HPMEC from female donors, open symbols represent HPMEC from male donors. *p value <0.05.

Figure 4. Results of proteomics analysis on HPMEC after shear stress in normoxia (Norm, 21% O_2) or hypoxia (Hypo, 1% O_2 for 24 hours). (A) Principal component analysis (PCA) of HPMEC. In a scatter plot of the first two principal components (Component 2 vs Component 1) the proteomic profile of each HPMEC sample is presented as a single symbol and coloured according to their experimental condition (black symbols - static normoxia, n=6; red symbols – static hypoxia, n=6, blue symbols - shear normoxia, n=6, green symbols – shear hypoxia, n=5). Individual donors are identified as male (M) or female (F) together with their age (years). Lines between points connect samples from an individual subject in normoxia and hypoxia. Samples segregate into static and sheared clusters according to Component 1 (separated by dotted curve). (B) Hierarchical clustering of 308 proteins found to have significantly different expression between HPMEC cultured in static conditions or shear stress in normoxia or hypoxia (FDR q value<0.05, ANOVA). (C) Heatmap showing a subset of the 308 proteins that were upregulated in response to hypoxia in both static and sheared conditions. (D) Heatmap showing a subset of the 308 proteins that were downregulated in response to hypoxia in both static and sheared conditions. High and low expression are shown in red and green respectively. Protein codes (Uniprot) were converted into gene names (HGNC) (Suppl. Tables 2 and 3). *FDR q value<0.05, ANOVA with Tukey's honestly significant difference (THSD) performed on ANOVA significant hits.

Figure 5. Heatmaps showing proteins (from the group of 308 proteins shown in Figure 4B) that changed in HPMEC in response to hypoxia (1% O_2 for 24 hours) in either static or sheared conditions but not both, detected using the proteomics analysis. (A) proteins that were upregulated in response to hypoxia only in static conditions. (B) proteins that were downregulated in response to hypoxia only in static conditions. (C) proteins that were upregulated in response to hypoxia only in sheared conditions. (D) proteins that were downregulated in response to hypoxia only in sheared conditions. High and low expression are shown in red and green respectively. For (A-D) *FDR q value<0.05, ANOVA with Tukey's honestly significant difference (THSD) performed on ANOVA significant hits. Protein codes (Uniprot) were converted into gene names (HGNC) (Suppl. Tables 4-7). "LMNA" Uniprot code

AJRCMB Articles in Press. Published February 02, 2023 as 10.1165/rcmb.2022-0340OC

is P02545, “LMNA ($)” Uniprot code is Q3BDU5. Black arrows indicate proteins that were plotted as representative examples of proteins from heatmaps (Figure 5C and 5D), thrombospondin 1 (THBS1) (E) and heat shock protein 90 (HSP90AA1) (F). LFQ, label-free quantification. For (E, F) data are presented as mean (SD), each symbol represents an individual donor. Solid symbols represent HPMEC from female donors, open symbols represent HPMEC from male donors. For (E, F) values were $\log_2$ transformed for calculation of P values (repeated measures ANOVA followed by the Holm-Šídák’s step-down test for pairwise comparisons). For (E, F) *p value <0.05.

Figure 6. The effect of shear stress and hypoxia (1% O_2 for 24 hours) on the markers of endothelial cell barrier integrity. (A) Junctional adhesion molecule A (JAM-A) also known as F11R, (B) F11R mRNA expression, (C) Tight junction protein 1 (TJP1), also known as ZO-1 protein, (D) TJP1 mRNA, (E) VE-cadherin (CDH5) protein and (F) CDH5 mRNA expression. (G) Immunofluorescent staining of ZO-1 (red). Nuclei were stained with DAPI (blue). White arrows indicate membrane localization. The scale bar corresponds to 10 µm (40x objective). For (A, C and E) protein expression was quantified by mass spectrometric analysis. LFQ, label-free quantification. (#) indicates that in this experimental group this protein was not detected in one of the subjects. P values were calculated using ANOVA and followed by the Holm-Šídák’s step-down test for pairwise comparisons. For statistical analysis of (B, D and F) normalized target gene expression was $\log_2$ transformed. P values were calculated using repeated measures ANOVA followed by the Holm-Šídák’s step-down test for pairwise comparisons. *p value <0.05. Data are presented as mean (SD), each symbol represents an individual donor. Solid symbols represent HPMEC from female donors, open symbols represent HPMEC from male donors.

Figure 7. Results of single cell RNA sequencing in lungs from healthy donors and lungs from patients with COPD from four publicly available datasets (10–13). (A) UMAP visualization of endothelial subtypes. (B) Heatmap of the top 15 differentially expressed genes (rows) for individual cells (columns) in each endothelial subtype. (C, D, E and F) Differentially expressed genes in general capillary cells and aerocytes that coded for proteins that were similarly changed in the proteomic analysis of HMPEC in response to hypoxia in sheared conditions. Males and females were compared separately: healthy females (Con, n=9) vs females with COPD (n=9) and healthy males (Con, n=12) vs males with COPD (n=7). (C) genes that increased in COPD and encoded proteins that also increased in response to hypoxia in both static and sheared conditions in HPMEC. (D) genes that increased in COPD and encoded proteins that increased in HPMEC in response to hypoxia only in sheared conditions. (E) genes that decreased in COPD and encoded proteins that decreased in HPMEC in response to hypoxia only in sheared conditions. Data are presented as violin plots, dots represent individual cells. General capillary cells female control, 692 cells. General capillary cells female COPD, 147 cells. General capillary cells male control, 166 cells. General capillary cells male COPD, 72 cells. Aerocytes female control, 256 cells. Aerocytes female COPD, 91 cells. Aerocytes male control, 60 cells. Aerocytes male COPD, 21 cells. Differentially expressed genes were identified using

AJRCMB Articles in Press. Published February 02, 2023 as 10.1165/rcmb.2022-0340OC

Wilcoxon two sample test with Bonferroni correction (*p-adjusted<0.05) and $\log_2$ difference >0.6 (1.5 fold-change). ns, p adjusted = 1.

AJRCMB Articles in Press. Published February 02, 2023 as 10.1165/rcmb.2022-0340OC

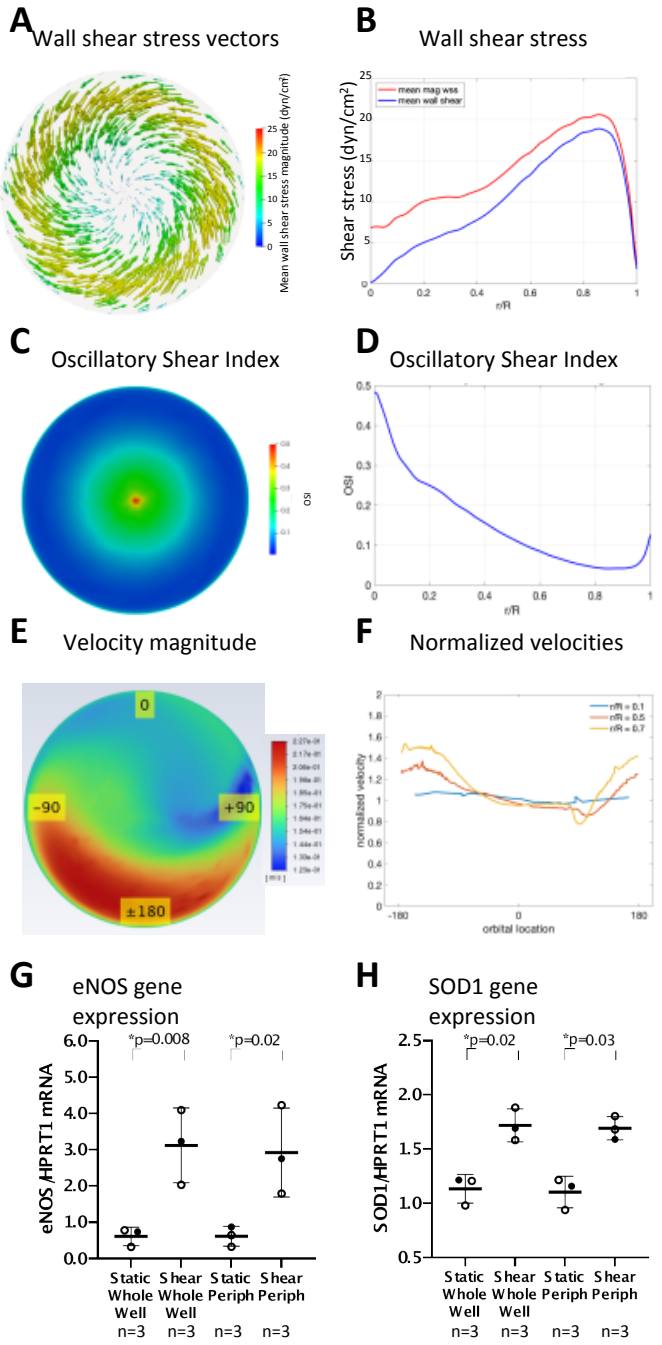

Figure 1

AJRCMB Articles in Press. Published February 02, 2023 as 10.1165/rcmb.2022-0340OC

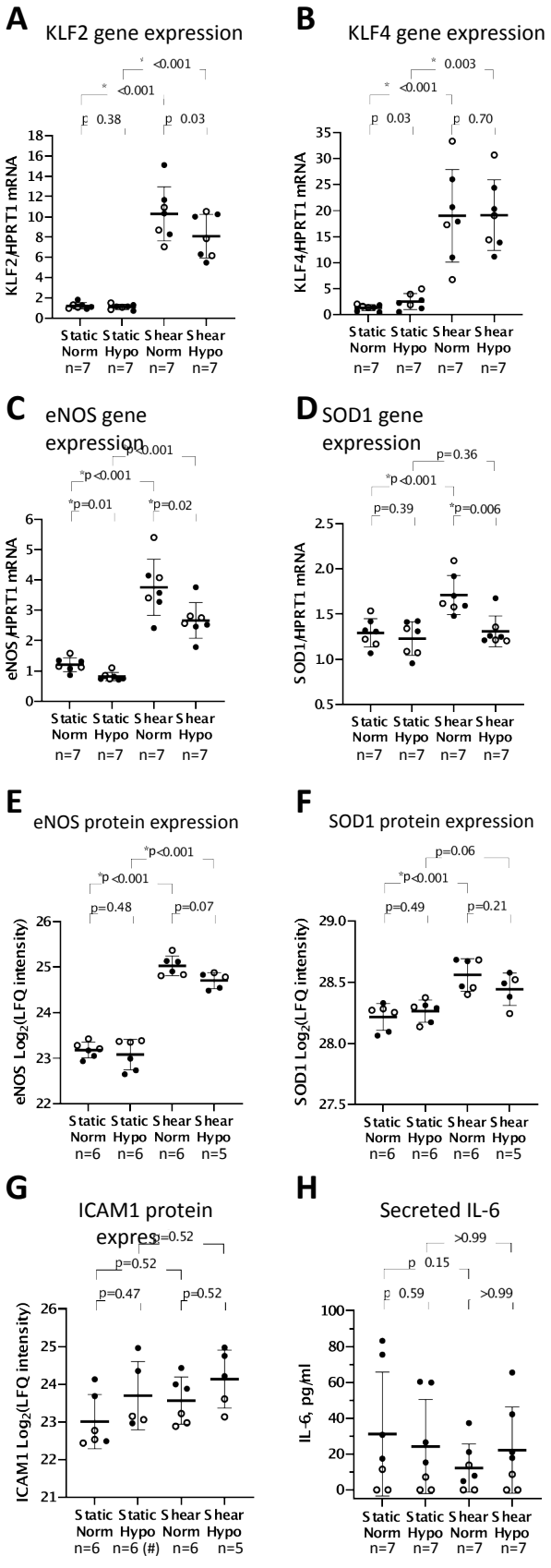

AJRCMB Articles in Press. Published February 02, 2023 as 10.1165/rcmb.2022-0340OC Figure 2

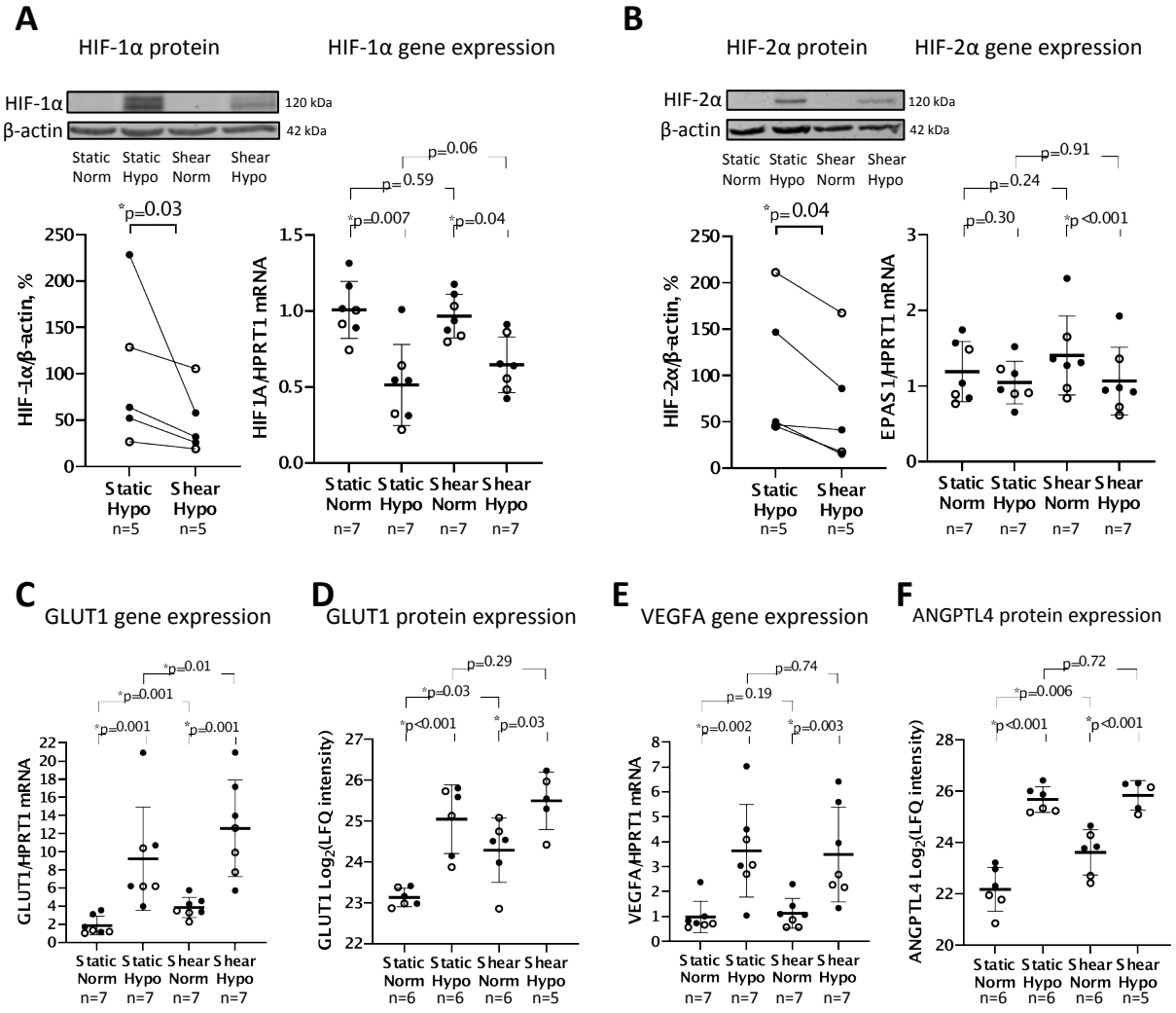

Figure 3

AJRCMB Articles in Press. Published February 02, 2023 as 10.1165/rcmb.2022-0340OC

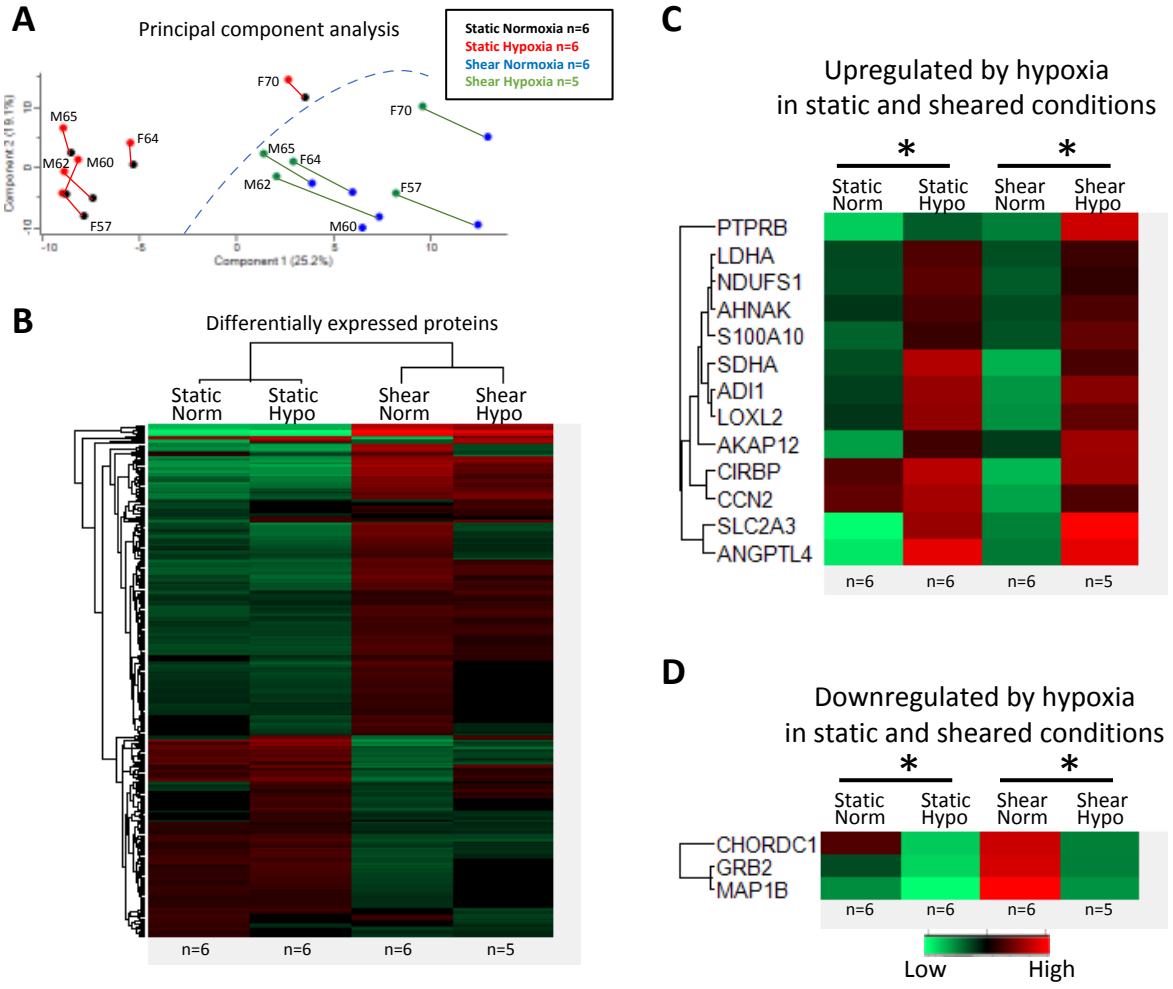

Figure 4

AJRCMB Articles in Press. Published February 02, 2023 as 10.1165/rcmb.2022-0340OC

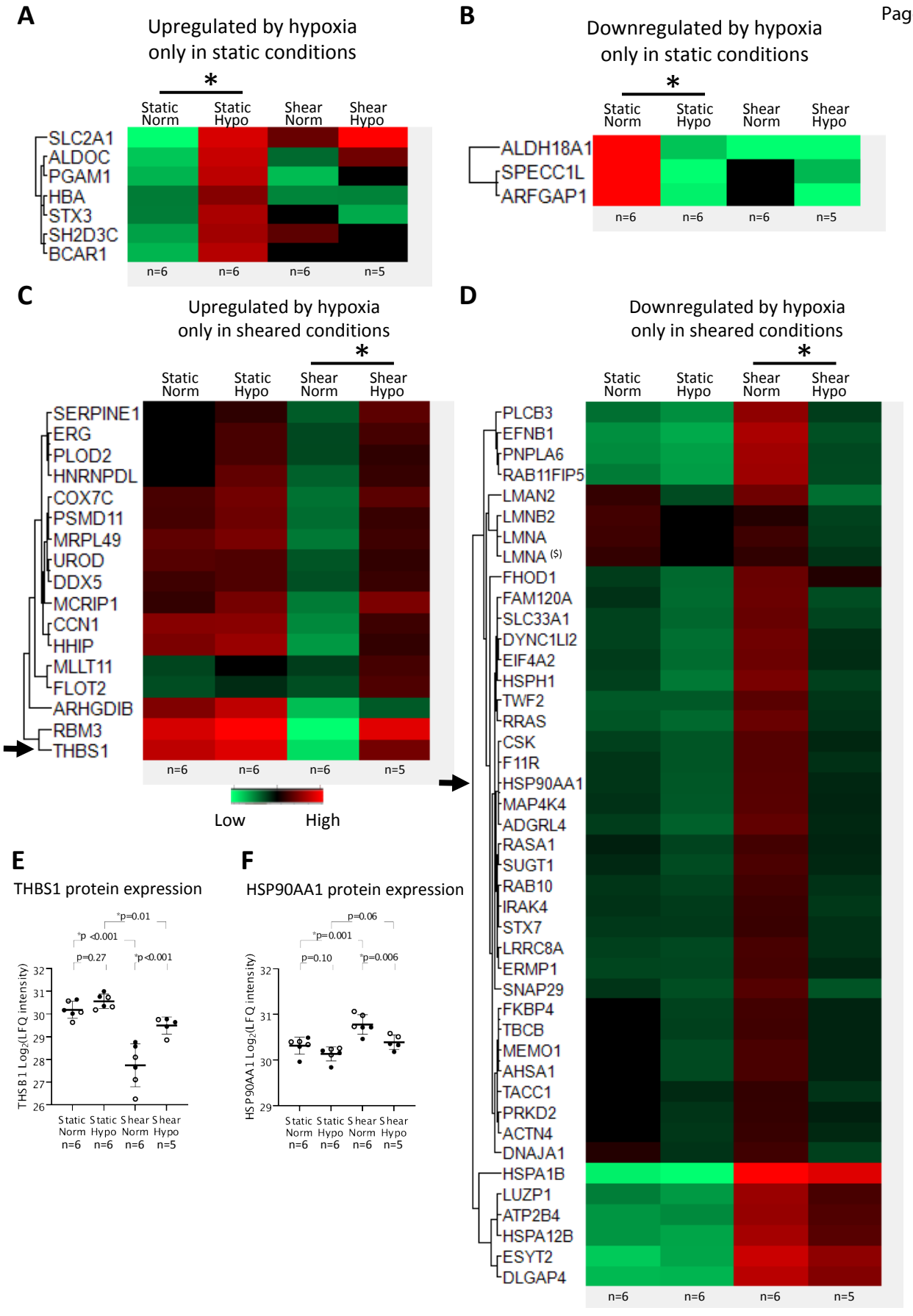

AJRCMB Articles in Press. Published February 02, 2023 as 10.1165/rcmb.2022-0348OC

Figure 5

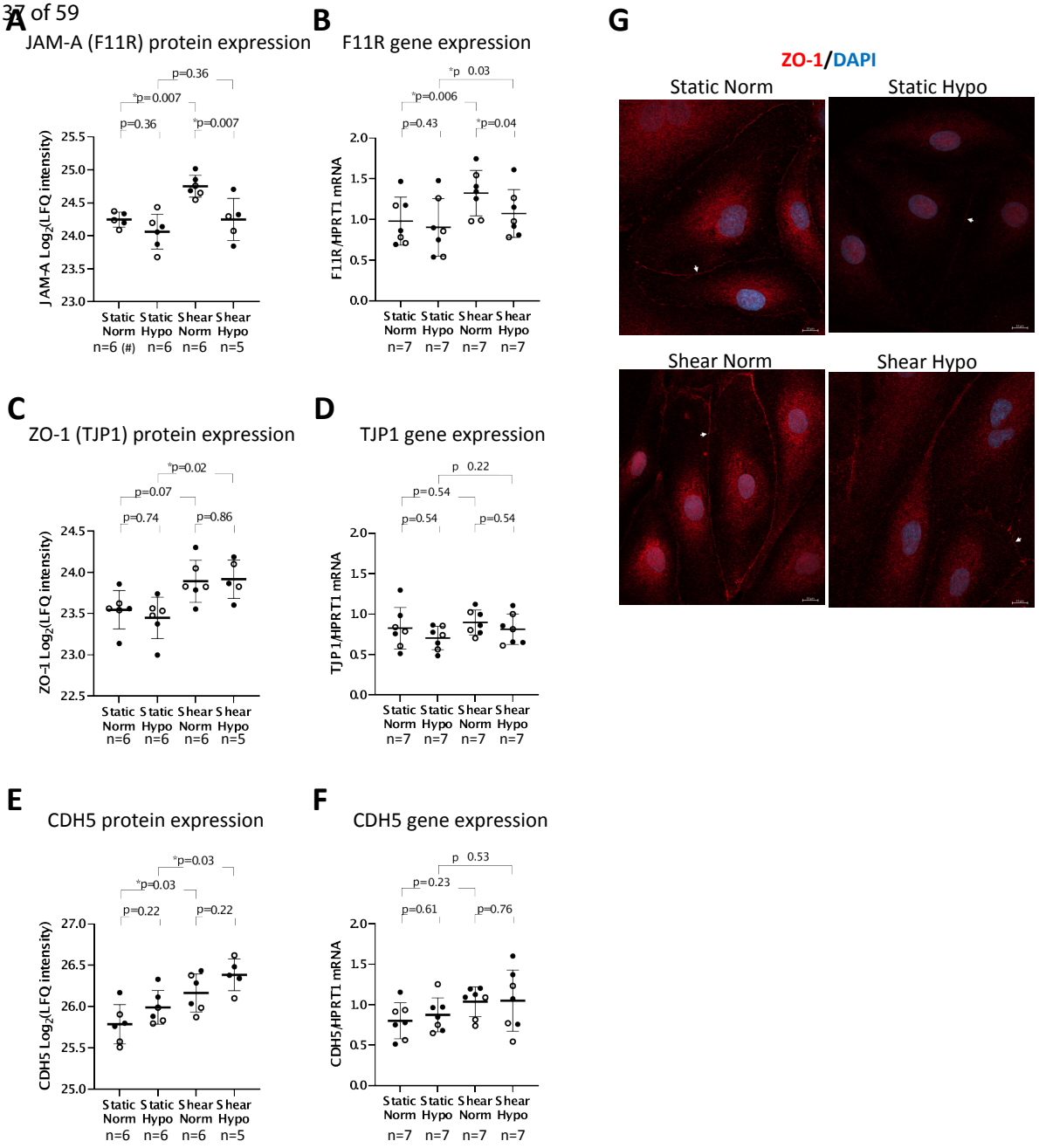

Figure 6

AJRCMB Articles in Press. Published February 02, 2023 as 10.1165/rcmb.2022-0340OC

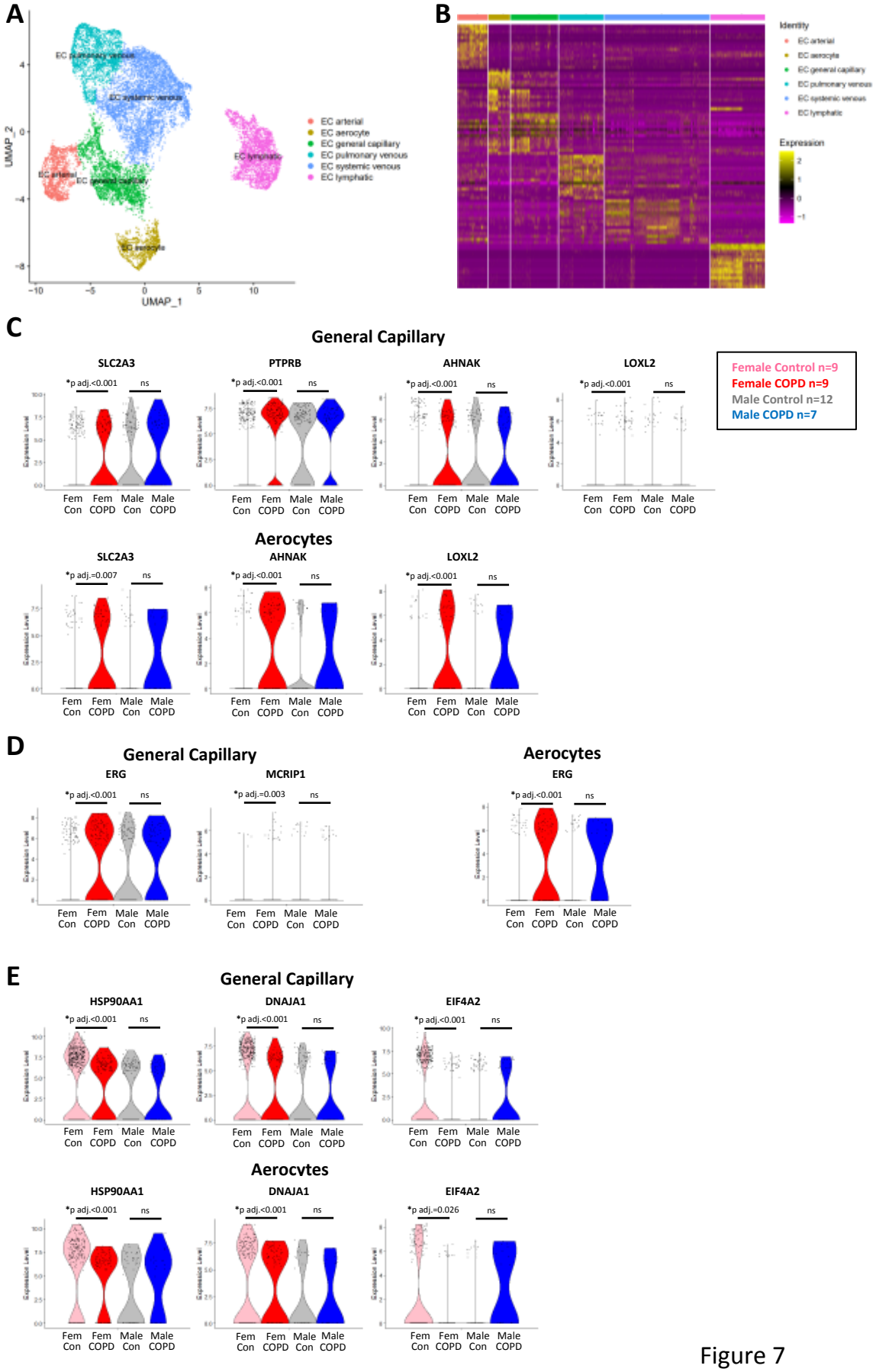

Figure 7

AJRCMB Articles in Press. Published February 02, 2023 as 10.1165/rcmb.2022-0340OC

Shear stress markedly alters the proteomic response to hypoxia in human pulmonary endothelial cells

Daria S. Kostyunina, Simon C. Rowan, Nikolai V. Pakhomov, Eugene Dillon, Keith D. Rochfort, Philip M. Cummins, Malachy J. O'Rourke, Paul McLoughlin

ONLINE DATA SUPPLEMENT

AJRCMB Articles in Press. Published February 02, 2023 as 10.1165/rcmb.2022-0340OC

Suppl. Methods

Shear stress application

Human pulmonary microvascular endothelial cells (HPMEC) from nine different healthy donors (four females and five males, 53-70 years old) were purchased (Promocell, Heidelberg, Germany) and grown in a standard medium MV2 (Promocell, Heidelberg, Germany) with Penicillin-Streptomycin 1% (Thermo Scientific, Waltham, USA).

HPMEC (passage 5) were seeded (9000 cells/cm^2) onto six well plates which had been precoated with 0.1% gelatine (Attachment Factor, Thermo Scientific, Waltham, USA). and grown in a standard tissue incubator (5%CO_2, 21%O_2) until 80-90% confluent.

To expose cells to shear stress, six well plates were placed on an orbital shaker (SSM1, Stuart, UK) (187 rotations per minute, radius of gyration 0.80 cm) and the relative viscosity of the cell culture medium was increased to 3.2 (measured using an Ostwald Viscometer) by addition of high molecular weight Ficoll® (7% Ficoll® PM400, Merck, Darmstadt, Germany) as previously described (1, 2). These conditions gave a shear stress of 10 dyn/cm^2 as calculated using a formula based on an extended solution to Stokes' second problem),

$$\tau = a\sqrt{\rho\mu(2\pi f)^3} \quad (1)$$

where a is the radius of gyration of the orbital shaker, ρ is medium density, μ is medium viscosity, f is frequency of rotation, an approach previously used to determine the shear stress experienced by cells cultured on an orbital shaker (1–3). We had previously shown that this produced optimal barrier function when compared to a lower level of shear stress (2). After 24 hours in these normoxic conditions, cells were either placed into hypoxic conditions

AJRCMB Articles in Press. Published February 02, 2023 as 10.1165/rcmb.2022-0340OC

(1% O_2 chamber, Coy Labs, Grass Lake, USA) or remained in normoxic conditions for a further 24 hours while shear stress continued.

Following 24 hours of hypoxia (and 48 hours of shear overall) HPMEC were lysed in buffer RLT™ (Qiagen, Germantown, USA) with 1 M DTT (Merck, Darmstadt, Germany) for RNA analysis or in RIPA buffer (Thermo Scientific, Waltham, USA) for protein analysis inside the hypoxic chamber. Separate cells were simultaneously cultured in standard static conditions in normoxia or hypoxia.

Computational Fluid Dynamics

Computational fluid dynamics (CFD) were used to characterise applied shear stress in detail. The parameters used for CFD were as follows: radius of gyration was 0.80 cm, radius of one well was 1.75 cm, the height of the medium in the well was 0.42cm, the medium viscosity was 0.00204 Ns/m^2 (high viscosity medium) or 0.00066 Ns/m^2 (standard viscosity medium), the medium density was 1023 kg/m^3 (high viscosity medium) or 998.5 kg/m^3 (standard viscosity medium), the frequency of rotation was 187 rotations per minute (high viscosity medium) or 275 rotations per minute (standard viscosity medium).

In general, the shear stress vector is given by

$$\vec{\tau} = \tau_x \hat{i} + \tau_y \hat{j} + \tau_z \hat{j} \quad (2)$$

Assuming that the surface of interest is an $x - y$ plane, the wall shear stress is determined at $z = 0$:

AJRCMB Articles in Press. Published February 02, 2023 as 10.1165/rcmb.2022-0340OC

$$\vec{\tau}_w(z=0) = \tau_w\hat{i} + \tau_y\hat{j} \quad (3)$$

The magnitude of the shear stress vector is given by

$$|\vec{\tau}_w| = \sqrt{\tau_x^2 + \tau_y^2} \quad (4)$$

There are two time averaged quantities to be considered the time average of wall shear stress and the time average of the magnitude of wall shear stress. The time average of wall shear stress is given by

$$TAWSS = \frac{1}{T}\int_0^T \vec{\tau}_w dt \quad (5)$$

The time average of the magnitude of the wall shear stress is given by

$$TAMWSS = \frac{1}{T}\int_0^T |\tau_w| dt \quad (6)$$

Oscillatory shear index is defined as

$$\text{OSI} = 0.5\left(1 - \frac{\left|\int_0^T \tau_w dt\right|}{\int_0^T |\tau_w| dt}\right) \quad (7)$$

The oscillatory shear index (OSI) describes shear stress acting in directions other than the direction of the mean shear stress vector i.e. multi-directional shear stress (4). *In vivo*, in areas of blood vessels with multi-directional shear stress, endothelial cells have cobble-stone appearance, are more permeable and express pro-inflammatory, pro-thrombothic and pro-oxidative genes (5, 6). OSI varies between a value of 0 and 0.5, 0 indicating unidirectional WSS throughout a complete rotation and 0.5 indicating purely oscillatory shear stress with a time-average of zero (4, 7).

AJRCMB Articles in Press. Published February 02, 2023 as 10.1165/rcmb.2022-0340OC

Determination of Mean Shear Stress

Transient data (shear stress), sampled at n equispaced discrete points along a single radius on the base of the well and extending over one period of revolution of the shaker, was exported from Ansys-Fluent to Matlab for post processing. A temporal average (5) yielded the radial distribution of the time-averaged wall shear stress. An area weighted average of this wall shear stress was then computed to yield the average wall shear stress on the base of the wall using equation (8)

$$\vec{\tau} = \frac{\sum_{k=1}^{n} TAWSS_k (2\pi r_k) \Delta \mathrm{r}}{\pi R^2} \tag{8}$$

where $\Delta r = R/n$

Numerical simulations were performed using Ansys 2021R2. The geometry of a single well was recreated in Ansys-Spaceclaim and imported in Ansys-Meshing. Mesh inflation was applied on both the bottom and side walls of the well. Following mesh independence studies the final computational mesh consisted of 1.05 million hexahedral elements. The mesh was then imported into Ansys-Fluent. The geometry was orientated with the $z-$ axis vertical, gravity applied in the $-z$ direction. The multiphase volume of fluid method was utilised to simulate the interaction between the two fluids in the simulation, the medium in the well and the ambient air. As the flow was turbulent, the k-ω Shear Stress Transport (SST) model was invoked, $y+$ values on the walls observed of order 1. The top surface of the well was specified as an outlet boundary condition with the pressure set at 0 Pa gauge (i.e. atmospheric pressure). The remaining boundary surfaces of the well were specified as no-slip wall boundary conditions. The well was rotated in the $x-y$ plane. Named expressions were used

AJRCMB Articles in Press. Published February 02, 2023 as 10.1165/rcmb.2022-0340OC

to specify the instantaneous u and v components of velocity calculated from the rotational speed *U* (=$R\omega$) and the period of rotation T as follows

$$u(t) = Ucos(\frac{2\pi t}{T}) \tag{8}$$

$$v(t) = Usin(\frac{3\pi t}{T}) \tag{9}$$

The coupled solver was utilised with default settings. All simulations were run for three rotations of the shaker initially ensuring that the calculation had become periodic. 1000 time steps per period of rotation were utilised. At each timestep, convergence was achieved when all residuals had fallen below 0.0001. The simulation was then run for one further rotation of the well during which time transient results were written to file for postprocessing in Paraview (Paraview-11.0) and Matlab (Matlab R2022a). Additionally, 'data sampling for time statistics', an option available within Ansys-Fluent, was used to average the flow field and obtain a time average of the velocity, pressure and stress fields. The outcome of this averaging process within Ansys-Fluent was compared with the same calculated from the transient data with Matlab. Excellent agreement was observed between the results.

Velocity vectors, normalised by rotational speed *U* (=$R\omega$) of the shaker were exported from Fluent to Matlab and plotted over the circumference at radii of 10%, 50% and 70% of the dish radius.

The Reynolds number Re was calculated as in (8) and given by

$$Re = \frac{\mathrm{HR2}\pi f\rho}{\mu} \tag{10}$$

where H is the height of fluid in the well, R is the well radius, f is the frequency of rotation, ρ is the fluid density, μ is the medium viscosity.

AJRCMB Articles in Press. Published February 02, 2023 as 10.1165/rcmb.2022-0340OC

The Froude number was calculated as in (8) and given by

$$Fr = \frac{\mathrm{R}2\pi f}{\sqrt{gH}} \quad (11)$$

Where R is the well radius, f is the frequency of rotation, g is the gravitational constant, and H is the height of the fluid.

RT-qPCR

Total RNA was extracted using columns (RNeasy Mini Kit, Qiagen, Germantown, USA) with on-column DNAse treatment (RNAse-Free DNase Set, Qiagen, Germantown, USA). RNA concentration was measured by Nanodrop 1000 (Thermo Scientific, Waltham, USA). Total RNA 1 (µg) was used for reverse transcription (SuperScript™ III, Invitrogen). RT-qPCR was undertaken using a thermocycler (QuantStudio 7 Flex, Thermo Scientific, Waltham, USA) using TaqMan probes (Thermo Scientific, Waltham, USA): KLF2 (Hs00360439_g1), KLF4 (Hs00358836_m1), NOS3 (eNOS) (Hs01574665_m1), SOD1 (Hs00533490_m1), HIF1A (Hs00153153_m1), EPAS1 (HIF2A) (Hs01026149_m1), SLC2A1 (GLUT1) (Hs00892681_m1), VEGFA (Hs00900055_m1), F11R (Hs00375889_m1), CDH5 (Hs00901465_m1), TJP1 (Hs01551871_m1). Analysis of RT-qPCR data was performed using the standard curve method. Target gene expression was normalized to housekeeping gene expression (HPRT1, Hs02800695_m1). HPMEC from seven donors (n=7) (three males and four females) were used for RT-qPCR. For statistical analysis normalized target gene expression was $\log_2$ transformed. P values were calculated using repeated measures one-way ANOVA with Geisser-Greenhouse correction and Holm-Šídák's multiple comparisons test (Prism 9, GraphPad, San Diego, USA).

AJRCMB Articles in Press. Published February 02, 2023 as 10.1165/rcmb.2022-0340OC

ELISA

Supernatant from cell culture plates was collected and stored at -80 °C until further analysis. IL-6 concentrations in supernatant were analysed using DuoSet ELISA for IL6 (lot P326914, DY406, R&D Systems, Minneapolis, MN) according to manufacturer's instructions. End-point values of samples and standards in duplicates were read by Clariostar (MBG Labtech, Germany). Quantification of IL-6 in samples was performed using extrapolation function of linear curve fit. P values were calculated using Friedman test with Dunn's correction for multiple comparisons (Prism 9, GraphPad, San Diego, USA).

Western Blotting

HPMEC protein lysates were centrifuged at 16000 g at 4°C for 15 minutes and supernatant was collected. Protein concentration was measured using BCA protein assay (Pierce™, Thermo Scientific, Waltham, USA). 12 µg of protein was mixed with LDS Sample Loading Buffer (4X) (G-Biosciences, St. Louis, USA) and Bolt™ Sample Reducing Agent (10X) (Invitrogen, Waltham, USA) and incubated at 70°C for 10 minutes for denaturation. Proteins were separated by electrophoresis in 8% gels (ProtoGel 30%, ProtoGel Stacking Buffer, ProtoGel Resolving Buffer 4X, National Diagnostics, Nottingham, UK) that was followed by transfer on polyvinylidene fluoride (PVDF) membrane, 0.45 µm pore size (Millipore, Merck, Darmstadt, Germany). The membranes were blocked with 5% skim milk (Millipore, Merck, Darmstadt, Germany) in TBS-T buffer for 1 hour at room temperature and incubated with primary antibodies at 4°C overnight. Primary antibodies used against: HIF-1α (1:1000, rabbit

AJRCMB Articles in Press. Published February 02, 2023 as 10.1165/rcmb.2022-0340OC

monoclonal, 36169S (D1S7W), lot 2, Cell Signaling, Beverly, USA), HIF-2α (1:1000, rabbit polyclonal, NB100-122SS, lot CO-3, Novus, Abington, UK), β-actin (1:5000, mouse monoclonal, A5441, lot 029M4883V, Merck, Darmstadt, Germany). The next day membranes were washed in Tris-buffered saline with 0.1% Tween 20 (TBS-T), incubated with secondary antibodies for 1 hour at room temperature, and washed in TBS-T again. The secondary antibodies used were as follows: goat anti-rabbit IgG (1:5000, DyLight™ 800, SA535571, lot TL277458, Invitrogen, Waltham, USA) and goat anti-mouse IgG (1:1000, DyLight™ 680, 35519, lot VB298075, Invitrogen, Waltham, USA). Protein was detected using fluorescence imaging system (Odyssey CLx, Li-Cor, Cambridge, UK) and quantified using Image Studio Lite software (Li-Cor, Cambridge, UK). Target protein expression was normalised to β-actin from the same sample. HPMEC from six donors were set to be used for protein analysis, however, there was insufficient protein available from one the sample of one subject, probably due to a technical error at the time of initial collection, so the final number of HPMEC donors for western blotting was five (n=5) (three females and two males). For statistical analysis normalised target protein expression was $\log_2$ transformed. P values were calculated using paired T-test (Prism 9, GraphPad, San Diego, USA).

Immunofluorescent imaging

HPMEC (from a male donor, 62 years old) were fixed in six well plates using 1 ml of 4% paraformaldehyde for 2 minutes at 37 °C, which were followed by 15 minutes of incubation

AJRCMB Articles in Press. Published February 02, 2023 as 10.1165/rcmb.2022-0340OC

at room temperature. Wells were washed with PBS and left at 4 °C covered with PBS for two days until staining was performed. For permeabilization cells were incubated with 1 ml/well of 0.2% saponin (S7900, Sigma) for 20 minutes at room temperature and then washed with PBS. For blocking cells were incubated with 1 ml/well of bovine serum albumin (BSA) (A21153, Sigma-Aldrich, Merck, Darmstadt, Germany) for 30 minutes at room temperature and then washed with PBS. Cells were incubated with primary antibodies tight junction protein 1 (ZO-1) (1:100, mouse monoclonal, ZO1-1A12, 33-9100, Thermo Scientific, Waltham, USA) in 5% BSA in PBS overnight at 4 °C. The next day antibody solution was removed, and cells were washed twice with PBS. Cells were incubated with goat anti-mouse IgG (1:500, DyLight™ 680, 35519, lot VB298075, Invitrogen, Waltham, USA) in 5% BSA in PBS for two hours at room temperature and washed twice with PBS. Nuclei were stained with DAPI (D9542, Sigma) 2 µg/ml for 3 minutes at room temperature. After washing, cells were mounted using Mowiol® 4-88 (81381, Sigma-Aldrich, Merck, Darmstadt, Germany) (1 hour at room temperature). Images were acquired using Zeiss microscope (Axio Imager Z2, LSM 800 confocal with Airy scan, Zeiss, Germany) at 40x magnification (C Plan-Apochromat 40x/1.30 objective). Identical settings were applied to acquire images from all four experimental conditions (static normoxia, static hypoxia, shear normoxia and shear hypoxia). Track 1 DyLight™ 680: pinhole - 5.00 AU/192µm, laser - 640 nm: 5.00 %, excitation - 691 nm, emission - 709 nm, detector gain - 900 V. Track 3 DAPI: pinhole - 5.41 AU/156 µm, laser - 405 nm: 0.4 %, excitation - 353 nm, emission - 465 nm, detector gain - 872 V. For all images white display was set to 400 for DyLight™680 and to 5000 for DAPI. Black was set to 0 and gamma was set to 1 for both channels.

AJRCMB Articles in Press. Published February 02, 2023 as 10.1165/rcmb.2022-0340OC

Mass spectrometry

The mass spectrometry proteomics data have been deposited to the ProteomeXchange Consortium via the PRIDE (9) partner repository with the dataset identifier PXD036260 and 10.6019/PXD036260.

For bottom-up proteomics, 25 µl of protein samples, lysed with RIPA, were mixed with 50 µl LYSE buffer (PreOmics, Munich, Germany), digested, and purified using columns (iST Sample Preparation Kit, PreOmics, Munich, Germany). The samples were analyzed by the Mass Spectrometry Resource (MSR) in University College Dublin on a mass spectrometer (Q Exactive, Thermo Scientific, Waltham, USA) connected to a chromatography system (Dionex Ultimate 3000, RSLCnano, Thermo Scientific, Waltham, USA). Peptides were separated on column, made of 3 µm C18-AQ Reprosil-Pur (Dr. Maisch, Tübingen, Germany) (length-100 mm; diameter-0.075 mm) over 120 min at a flow rate of 250 nL/min with a linear gradient of increasing ACN from 1% to 27%. The mass spectrometer was operated in data dependent mode; α high resolution (70,000) MS scan (300-1600 m/z) was performed to select the twelve most intense ions and fragmented using high energy C-trap dissociation for MS/MS analysis.

Data processing and Bioinformatics

Raw data from the mass spectrometer was processed using the MaxQuant software (version 2.0.3.0) incorporating the Andromeda search engine (10–12). To identify peptides and proteins, MS/MS spectra were matched against Uniprot homo sapiens database (2021_03) containing 78,120 entries. All searches were performed using the default setting of MaxQuant, with trypsin as specified enzyme allowing two missed cleavages and a false discovery rate of 1% on the peptide and protein level. The database searches were performed with carbamidomethyl (C) as fixed modification and acetylation (protein N terminus) and

AJRCMB Articles in Press. Published February 02, 2023 as 10.1165/rcmb.2022-0340OC

oxidation (M) as variable modifications. For the generation of label free quantitative (LFQ) ion intensities for protein profiles, signals of corresponding peptides in different nano-HPLC MS/MS runs were matched by MaxQuant in a maximum time window of 1 min (13). Statistical analysis of proteomic data was undertaken in Perseus software (version 1.6.2.3) according to the developer's protocol (14, 15). Differentially expressed proteins (ANOVA, permutation-based FDR with 250 randomisations, q value<0.05) were identified. Tukey's honestly significant difference (THSD) test was performed on ANOVA significant hits. Where expression of specific individual proteins was examined, P values were calculated using ANOVA and followed by the Holm-Šídák's step-down test for pairwise comparisons.

Single cell RNA-sequencing

Four publicly available datasets from the GEO database were used for single cell RNA-sequencing analysis (16–19). Analysis was undertaken in R (version 4.0.3(2020-10-10)) using Seurat version 4.0.0 (MAST version 1.15.0) (20). Endothelial cells were identified as cells prominently expressing canonical markers such as vWF, PECAM1, CLDN5 as well the markers reported by the authors of the source datasets. Quality control (QC) was undertaken on each individual dataset: percentage of mitochondria genes ("percent.mt"), the number of read counts ("nCount_RNA") and number of genes ("nFeature_RNA") were visualised using violin plots and outliers were removed.

The endothelial cell subsets from each dataset were integrated using the "SCTransform" methodology which replaces the NormalizeData, ScaleData and FindVariableFeature steps in the standard workflow. During normalization, mitochondrial mapping percentage, a confounding source of variation, was removed. To integrate datasets integration anchors

AJRCMB Articles in Press. Published February 02, 2023 as 10.1165/rcmb.2022-0340OC

were identified with the “FindIntegrationAnchors”. Normalization method was set to “SCT”. Principal components were calculated using the “RunPCA” in JackStraw (result suggested PC8/9) and Elbow plot (result suggested PC8/9 with full flat line at PC15) methods. Visualisation and clustering were undertaken on the integrated dataset. Based on JackStraw and Elbow plot the K-nearest neighbour and clusters for various resolutions were determined. UMAP with selected resolutions was run to visualise cell distribution after the integration (Suppl. Fig. 2). Gene clusters (cell subtypes) were identified using “FindAllMarkers” command. Endothelial cell (EC) subtypes were identified using previously reported gene markers (21): EC systemic venous (ZNF385D, COL15A1, TPD52L1), EC lymphatic (LYVE1, PDPN, CCL21, SEMA3D), EC general capillary (FCN3, IL7R, RGCC, SCL6A4), EC pulmonary venous (CPE, CLU, C7, ACKR1, IGFBP7), EC arterial (DKK2, IGFBP3, SERPINE2), EC aerocyte (SOSTDC1, EDNRB, CA4, S100A4) (Figure 7A). A small contaminating cluster identified as immune cells (FCER1G, LYZ, CD68, MRC1 gene markers) was excluded. QC metrics - percentage of mitochondria genes (“percent.mt”), the number of read counts (“nCount_RNA”) and number of genes (“nFeature_RNA”), were visualised using violin plots (Suppl. Figure 3). Differentially expressed gene markers for each subtype were identified using MAST and the heatmap on the top 15 genes was generated (Figure 7B).

The integrated EC dataset contained cells from IPF donors (17–19) (Suppl. Figure 2). These cells were identified and excluded from further analysis (Suppl. Figure 2). For the final analysis we identified the ECs from donors that were age-matched (50-76 years old) to the donors of the HPMEC used in our *in vitro* studies. We set a threshold to include male donors >50 years old and female donors > 55 years old. Final single cell RNA-sequencing donor numbers were: 21 control donors (12 males and 9 females) and 16 donors with COPD (7 males and 9 females) only. Differentially expressed genes (DEGs) between COPD and control cells were identified

AJRCMB Articles in Press. Published February 02, 2023 as 10.1165/rcmb.2022-0340OC

using MAST framework with “min.pct = 0.10” i.e., 10% of cells had to express the gene in either the control or COPD datasets. DEGs were considered to be significant if P adjusted was less than 0.05, calculated using Wilcoxon two sample test with Bonferroni correction.

Because COPD leads to alveolar hypoxia (58) we focused on two types of alveolar endothelial cells, aerocytes, which are responsible for gas exchange, and general capillary cells, which are precursors of aerocytes and release vasoactive substances (22). The numbers of general capillary cells and aerocytes from these aged match control and COPD donors were 1077 cells, and 428 cells respectively. Among general capillary cells 692 cells were in a female control group, 147 cells were in female COPD, 166 cells were in male control and 72 cells were in male COPD. In a female control group, there were 256 aerocytes, in female COPD 91 aerocytes, in male control 60 aerocytes, in male COPD 21 aerocytes.

Data availability

Published datasets of single cell RNA sequencing data on human lung GSE128169 (16), GSE128033 (17), GSE136831 (18), GSE122960 (19).

AJRCMB Articles in Press. Published February 02, 2023 as 10.1165/rcmb.2022-0340OC

Supplemental Table 1. Comparison between standard and high viscosity medium.

Medium	Rotation frequency, rotations per minute	Density, kg/m^3	Viscosity, NS/m^2	Shear stress according to equation (1), dyn/cm^2	Mean shear stress according to CFD, dyn/cm^2	Reynolds Number	Froude number
High viscosity medium	187	1023	0.00204	10.02	13.1	721	1.69
Standard medium	275	998.5	0.00066	10.01	14.36	3221	2.48

Notes. The radius of gyration of the orbital shaker was 0.8 cm, the radius of each well was 1.75 cm, the height of the culture medium in the well was 0.42 cm. CFD-computational fluid dynamics.

AJRCMB Articles in Press. Published February 02, 2023 as 10.1165/rcmb.2022-0340OC

Online supplement references

1. Ley K, Lundgren E, Berger E, Arfors K. Shear-dependent inhibition of granulocyte adhesion to cultured endothelium by dextran sulfate. *Blood* 1989;73:1324–1330.

2. Rowan SC, Rochfort KD, Piouceau L, Cummins PM, O'Rourke M, McLoughlin P. Pulmonary endothelial permeability and tissue fluid balance depend on the viscosity of the perfusion solution. *Am J Physiol Cell Mol Physiol* 2018;315:L476–L484.

3. Colgan OC, Ferguson G, Collins NT, Murphy RP, Meade G, Cahill PA, Cummins PM. Regulation of bovine brain microvascular endothelial tight junction assembly and barrier function by laminar shear stress. *Am J Physiol - Hear Circ Physiol* 2007;292:3190–3197.

4. Ku DN, Giddens DP, Zarins CK, Glagov S. Pulsatile flow and atherosclerosis in the human carotid bifurcation. Positive correlation between plaque location and low oscillating shear stress. *Arterioscler Thromb Vasc Biol* 1985;5:293–302.

5. Hahn C, Schwartz MA. Mechanotransduction in vascular physiology and atherogenesis. *Nat Rev Mol Cell Biol* 2009;10:53–62.

6. Wu D, Birukov K. Endothelial Cell Mechano-Metabolomic Coupling to Disease States in the Lung Microvasculature. *Front Bioeng Biotechnol* 2019;7:1–18.

7. Ghim M, Pang KT, Arshad M, Wang X, Weinberg PD. A novel method for segmenting growth of cells in sheared endothelial culture reveals the secretion of an anti-inflammatory mediator. *J Biol Eng* 2018;12:1–13.

8. Thomas JMD, Chakraborty A, Berson RE. Validation of a CFD Model of an Orbiting Culture Dish with PIV and Analytical Solutions. *AIChE J* 2017;63:4233–4242.

9. Perez-Riverol Y, Bai J, Bandla C, García-Seisdedos D, Hewapathirana S, Kamatchinathan S, Kundu DJ, Prakash A, Frericks-Zipper A, Eisenacher M, Walzer M, Wang S, Brazma A, Vizcaíno JA. The PRIDE database resources in 2022: A hub for mass spectrometry-based proteomics evidences. *Nucleic Acids Res* 2022;50:D543–D552.

10. Cox J, Mann M. MaxQuant enables high peptide identification rates, individualized p.p.b.-range mass accuracies and proteome-wide protein quantification. *Nat Biotechnol* 2008;26:1367–1372.

11. Tyanova S, Temu T, Cox J. The MaxQuant computational platform for mass spectrometry-based shotgun proteomics. *Nat Protoc* 2016;11:2301–2319.

12. Cox J, Neuhauser N, Michalski A, Scheltema RA, Olsen J V., Mann M. Andromeda: A peptide search engine integrated into the MaxQuant environment. *J Proteome Res* 2011;10:1794–1805.

13. Cox J, Hein MY, Luber CA, Paron I, Nagaraj N, Mann M. Accurate proteome-wide label-free quantification by delayed normalization and maximal peptide ratio extraction, termed MaxLFQ. *Mol Cell Proteomics* 2014;13:2513–2526.

14. Tyanova S, Temu T, Sinitcyn P, Carlson A, Hein MY, Geiger T, Mann M, Cox J. The Perseus computational platform for comprehensive analysis of (prote)omics data. *Nat Methods* 2016;13:731–740.

15. Tyanova S, Cox J. Perseus: A Bioinformatics Platform for Integrative Analysis of Proteomics Data in Cancer Research. *von Stechow L Cancer Syst Biol Methods Mol Biol* 2018. p. 133–148.

16. Valenzi E, Bulik M, Tabib T, Morse C, Sembrat J, Trejo Bittar H, Rojas M, Lafyatis R. Single-cell

AJRCMB Articles in Press. Published February 02, 2023 as 10.1165/rcmb.2022-0340OC

analysis reveals fibroblast heterogeneity and myofibroblasts in systemic sclerosis-associated interstitial lung disease. *Ann Rheum Dis* 2019;78:1379–1387.

17. Morse C, Tabib T, Sembrat J, Buschur KL, Bittar HT, Valenzi E, Jiang Y, Kass DJ, Gibson K, Chen W, Mora A, Benos P V., Rojas M, Lafyatis R. Proliferating SPP1/MERTK-expressing macrophages in idiopathic pulmonary fibrosis. *Eur Respir J* 2019;54:.

18. Adams TS, Schupp JC, Poli S, Ayaub EA, Neumark N, Ahangari F, Chu SG, Raby BA, DeIuliis G, Januszyk M, Duan Q, Arnett HA, Siddiqui A, Washko GR, Homer R, Yan X, Rosas IO, Kaminski N. Single-cell RNA-seq reveals ectopic and aberrant lung-resident cell populations in idiopathic pulmonary fibrosis. *Sci Adv* 2020;6:.

19. Reyfman PA, Walter JM, Joshi N, Anekalla KR, McQuattie-Pimentel AC, Chiu S, Fernandez R, Akbarpour M, Chen CI, Ren Z, Verma R, Abdala-Valencia H, Nam K, Chi M, Han SH, Gonzalez-Gonzalez FJ, Soberanes S, Watanabe S, Williams KJN, Flozak AS, Nicholson TT, Morgan VK, Winter DR, Hinchcliff M, Hrusch CL, Guzy RD, Bonham CA, Sperling AI, Bag R, *et al.* Single-cell transcriptomic analysis of human lung provides insights into the pathobiology of pulmonary fibrosis. *Am J Respir Crit Care Med* 2019;199:1517–1536.

20. Hao Y, Hao S, Andersen-Nissen E, Mauck WM, Zheng S, Butler A, Lee MJ, Wilk AJ, Darby C, Zager M, Hoffman P, Stoeckius M, Papalexi E, Mimitou EP, Jain J, Srivastava A, Stuart T, Fleming LM, Yeung B, Rogers AJ, McElrath JM, Blish CA, Gottardo R, Smibert P, Satija R. Integrated analysis of multimodal single-cell data. *Cell* 2021;184:3573-3587.e29.

21. Schupp JC, Adams TS, Cosme C, Raredon MSB, Yuan Y, Omote N, Poli S, Chioccioli M, Rose KA, Manning EP, Sauler M, Deiuliis G, Ahangari F, Neumark N, Habermann AC, Gutierrez AJ, Bui LT, Lafyatis R, Pierce RW, Meyer KB, Nawijn MC, Teichmann SA, Banovich NE, Kropski JA, Niklason LE, Pe'er D, Yan X, Homer RJ, Rosas IO, *et al.* Integrated Single-Cell Atlas of Endothelial Cells of the Human Lung. *Circulation* 2021;286–302.doi:10.1161/CIRCULATIONAHA.120.052318.

22. Gillich A, Zhang F, Farmer CG, Travaglini KJ, Tan SY, Gu M, Zhou B, Feinstein JA, Krasnow MA, Metzger RJ. Capillary cell-type specialization in the alveolus. *Nature* 2020;586:785–789.

AJRCMB Articles in Press. Published February 02, 2023 as 10.1165/rcmb.2022-0340OC

Suppl. Figure 1. Shear stress which cells would have experienced if standard (low viscosity) cell culture medium was used and the rotation frequency increased to produce a shear stress identical to that used in the experiments we report, as calculated using the formula based on an extended solution to Stokes' second problem (10 dyn/cm^2), a commonly used approach. (A and B) Computational fluid dynamics, calculated for a well in a six-well plate, rotated on an orbital shaker (rotation frequency - 275 rpm, radius of gyration - 0.8 cm, radius of well - 1.75 cm, medium volume - 4 ml, relative medium viscosity – 1.1, density of medium 998.5 kg/m^3). (A) Mean wall shear stress vectors within a well and wall shear stress (red curve - time average of the magnitude of the shear stress; blue curve - time average of the wall shear stress vectors). (B) Oscillatory Shear Index. Note the much larger area that would have experienced a high mean magnitude of shear stress and high OSI that in our method using a high viscosity medium (markedly reduced area of high mean magnitude of shear stress and reduced area of high OSI).

Suppl. Figure 2. UMAP showing the successful integration of single cell RNA-sequencing datasets from healthy and COPD lungs.

Suppl. Figure 3. Violin plots of quality control metrics: percentage of mitochondrial genes "percent.mt", number of read counts ("nCount_RNA") and number of genes ("nFeature_RNA") in endothelial cell subtypes after integration.

AJRCMB Articles in Press. Published February 02, 2023 as 10.1165/rcmb.2022-0340OC

A

Wall Shear Stress

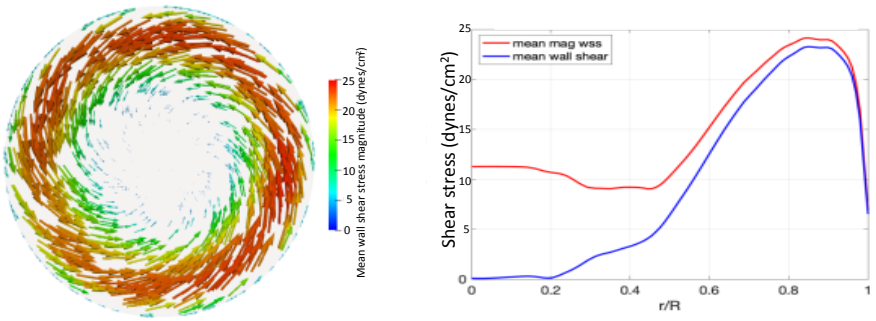

B

Oscillatory Shear Index

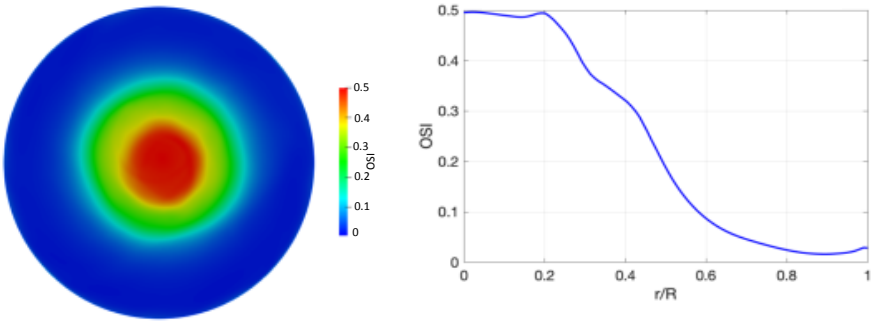

Supplementary Figure 1

AJRCMB Articles in Press. Published February 02, 2023 as 10.1165/rcmb.2022-0340OC

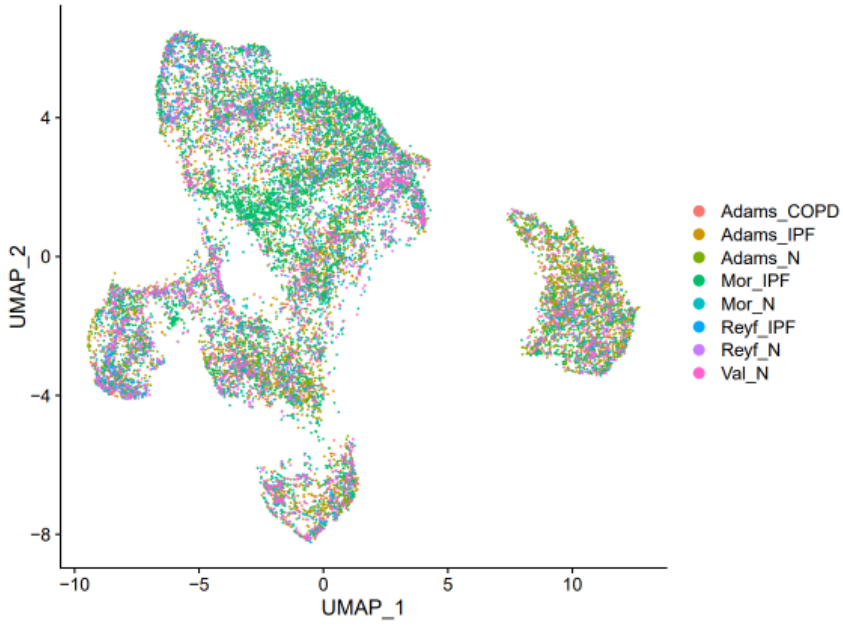

Supplementary Figure 2

AJRCMB Articles in Press. Published February 02, 2023 as 10.1165/rcmb.2022-0340OC

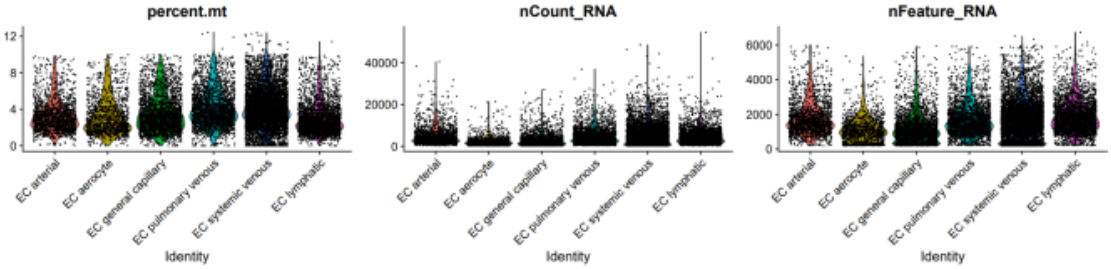

Supplementary Figure 3

AJRCMB Articles in Press. Published February 02, 2023 as 10.1165/rcmb.2022-0340OC